MODELING OF RADICAL–SURFACE INTERACTIONS IN THE PLASMA-ENHANCED CHEMICAL VAPOR DEPOSITION OF SILICON THIN FILMS

Dimitrios Maroudas

Department of Chemical Engineering, University of California, Santa Barbara, Santa Barbara, California 93106-5080

ADVANCES IN CHEMICAL ENGINEERING, VOL. 28 0065-2377/01 $35.00

I. Introduction

Growth of thin films by plasma-enhanced chemical vapor deposition (PECVD) enables a wide range of technologies for manufacturing electronic, optoelectronic, and photovoltaic devices (Reif, 1990; Crowley, 1992; Sinke, 1993). The use of highly reactive gas plasmas in PECVD allows for growth of thin films at temperatures that are much lower than those needed for other (CVD) processes (Randhawa, 1991; Graves, 1994; Smith, 1996). This ability to deposit films at low temperatures is due to the highly nonequilibrium environment of the gas discharge that leads to generation of ions and chemically reactive radicals through, e.g., electron impact dissociation. In spite of the widespread use of PECVD, process optimization and reactor design rely on completely empirical procedures that are not transferable among different reactor types or chemical systems. However, advances in plasma processing applications to surpass existing technological limits require a fundamental understanding of plasma physics and homogeneous and heterogeneous plasma chemistry, as well as species transport in plasma reactors (Graves *et al.,* 1996).

Among the least understood aspects of plasma processing technologies are plasma–surface interactions, i.e., phenomena occurring on the growth surface upon impingement of chemically reactive radicals and energetic species from the plasma (Graves *et al.,* 1996). The absence of a fundamentally based framework of surface reaction kinetics and its integration with species transport and reaction kinetics in the gas phase is a long-standing problem that limits the predictive capabilities of plasma reactor models (Proud *et al.,* 1991; Graves *et al.,* 1996). Typically, plasma modeling studies treat surface reactions in a phenomenological manner, accounting only for the presence of the surface and its effects on the gas-phase species concentrations through lumped surface reaction kinetics. However, development of predictive plasma reactor models requires detailed information on the reactions of species impinging on the surface from the plasma (Maroudas and Shankar, 1996).

Systematic investigations of plasma–surface interactions under realistic PECVD conditions require knowledge of fluxes and energies of species incident onto the surface from the plasma, structure and composition of the deposition surface, and elementary reaction processes that produce the surface species from the radicals and ions that impinge on the surface. Although the surface composition and species fluxes and energies can be determined experimentally through simultaneous use of plasma and surface diagnostics, surface reaction processes cannot be observed directly during deposition. This problem, however, can be addressed by atomic-scale simulation

methods, which provide ideal means for detailed nanoscopic modeling of the interactions of radicals and molecular fragments from the plasma with surfaces, as well as determination of surface reaction mechanisms and kinetics.

PECVD from silane (SiH_4) and hydrogen (H_2) containing discharges is used widely for the production of hydrogenated amorphous silicon (a-Si:H) and nanocrystalline silicon (nc-Si:H). Thin films of these materials have numerous industrial applications ranging from solar cells to the manufacturing of thin-film transistors for flat panel displays (Crowley, 1992; Sinke, 1993). The identities and the fluxes of chemically reactive species that originate in the plasma and impinge onto the deposition surface determine the structural quality and, therefore, the electronic properties of the deposited films. Experimental research on silicon plasma deposition has provided empirical ranges of processing conditions, such as substrate temperatures and feed gas composition, for improving the structural quality of the PECVD-grown films (see, e.g., Abelson, 1993). However, even after decades of research into the growth of these silicon thin films, the reaction mechanisms between the species from the gas phase and the deposition surface, as well as the kinetics of these surface reactions remain largely unknown; even the identities of the deposition precursors are still under debate (Abelson, 1993).

This article presents an integrated atomic-scale computational methodology for the fundamental mechanistic and quantitative understanding of plasma–surface interactions that govern the plasma-assisted deposition of thin films. The article focuses on the growth of silicon thin films and, in particular, a-Si:H films. PECVD of Si films is viewed as an ideal prototypical system: in spite of its own technological importance, the study of this system can be used to examine and develop modeling tools and strategies that can be transferable to a wide class of materials processing systems. Among the various types of species generated in the discharge, this article places special emphasis on chemically reactive radicals. Recent progress in modeling radical–surface interactions in the plasma deposition of a-Si:H films is reviewed: radical–surface interactions are identified, reaction mechanisms are elucidated, reaction energetics are analyzed, and computationally deposited a-Si:H films are characterized. In spite of the focus of this article on radicals, the important roles of the ions impinging on the surface in modifying the near-surface region is realized: energetic ions can cause surface sputtering and induce various surface reactions, such as desorption reactions. The role of such ions in the surface structural and chemical characteristics of the computationally deposited films also is discussed briefly. Given that even the computational generation of a realistic amorphous network remains an open research subject, addressing the above problems rigorously at the atomic scale is a very challenging task. Integration of the resulting knowledge of plasma–surface chemistry into a reactor-scale description with

predictive capabilities for process optimization is even more challenging. Chemical engineering contributions in this area can have major impact on microelectronics and other electronic device fabrication technologies.

II. Computational Methodology

Atomic-scale theoretical studies can contribute significantly to our fundamental and quantitative understanding of plasma–surface interactions and the development of an accurate chemical reaction database that is critical for progress in plasma process modeling. Quantitative accuracy in the analysis of plasma–surface interactions is guaranteed only by first-principles quantum mechanical (QM) calculations, i.e., *ab initio* calculations of the electronic structure for given atomic positions and the forces on the atoms when displaced from their equilibrium configuration (Car and Parrinello, 1985; Payne *et al.,* 1992). Such accurate calculations are limited to small clusters of atoms, or small periodic supercells that contain up to a hundred (or a few hundreds of) atoms, and integration of the equations of atomic motion over a few picoseconds. Plasma–surface interactions, however, are characterized by a much broader range of length and time scales. Thus, addressing the problem theoretically based solely on accurate QM calculations is computationally impractical. In spite of the continuous increase in computational power that will enable QM calculations over larger length scales and longer time scales, parametric studies at this level of theory will remain impractical. On the other hand, targeted accurate QM analysis of surface reactions is computationally feasible (Ricca and Musgrave, 1999; Ramalingam *et al.,* 1998c) for the development of databases of energetic and kinetic reaction parameters.

Atomistic simulation methods based on classical force fields provide computationally efficient means for the investigation of nanoscopic mechanisms that determine the interactions between surfaces and chemically reactive species from a plasma. These methods include molecular-statics (MS), Monte Carlo (MC), and molecular-dynamics (MD) techniques (Abraham, 1986; Ciccotti *et al.,* 1987; Allen and Tildesley, 1990; Maroudas and Brown, 1993; Rapaport, 1998). Combination of these techniques allows for monitoring of dynamical phenomena, analysis of reaction paths, and relaxation of the surface structure. Fundamental mechanistic understanding gained by such simulations can provide the necessary insights to guide efficiently parametric studies and design of experimental protocols. These simulations, however, are limited by the accuracy of the classical interatomic potential used to calculate the total energy and the resulting interatomic forces. Fully empirical parametrization of classical force fields is not transferable to widely different physicochemical environments. The transferability of such force

fields can be improved substantially by systematic parametrization schemes based on accurate QM-calculated energy surfaces, including energy landscapes for radical–surface interactions.

Regardless of the accuracy and transferability of a classical force field, dynamical simulations based on MD techniques are limited to time scales of the order of nanoseconds. However, these time scales that can be captured directly by MD are shorter by orders of magnitude than the actual time scales characteristic, e.g., of surface relaxation phenomena during a surface growth process. In spite of recent progress in accelerating the MD simulation of infrequent events (Voter, 1997a,b; 1998; Pal and Fichthorn, 1999), kinetic MC (KMC) simulation methods provide the most practical approach to overcome time-scale limitations in complex chemically reactive systems. Such KMC methods can extend the propagation of the dynamical system to time scales longer by several orders of magnitude than those that can be captured directly by MD within an atomic-scale description of the physicochemical process (Limoge and Bocquet, 1988; Kang and Weinberg, 1989; Fichthorn and Weinberg, 1991). The inherent limitation of KMC methods is that their accuracy depends fully on the completeness and accuracy of the database of transition probabilities that is used as input to KMC simulations: the development of such an accurate database for a complex physicochemical process is a particularly challenging task.

Over the past decade, atomic-scale simulation based on MD and KMC techniques has been applied extensively to study deposition processes, most notably semiconductor epitaxial growth (Srivastava and Garrison, 1990, 1991; Crowley *et al.,* 1993) and diamond film growth (Dawnkaski *et al.,* 1996; Battaile *et al.,* 1997; 1998). In the area of plasma–surface interactions, atomic-scale simulations have focused mostly on understanding sputtering and etching processes on silicon surfaces exposed to various discharges (Schoolcraft and Garrison, 1991; Weakliem and Carter, 1993; Barone and Graves, 1995a,b; Helmer and Graves, 1997, 1998, 1999; Kubota *et al.,* 1998; Kubota and Economou, 1999; Kim *et al.,* 1999; Hanson *et al.,* 1999; Srivastava *et al.,* 1999; Halicioglu and Srivastava, 1999). In addition, substantial simulation effort has been devoted recently to the understanding and analysis of interactions between Si surfaces and chemically reactive species from silane-containing plasmas (Ramalingam *et al.,* 1998a–c, 1999a–c, 2000).

A. The Hierarchical Approach

The advantages of accuracy and computational efficiency of the different levels of theory outlined above can be realized through a hierarchical computational approach that links QM calculations with MS/MC/MD and KMC simulations. Such a hierarchical approach is illustrated in Fig. 1. The

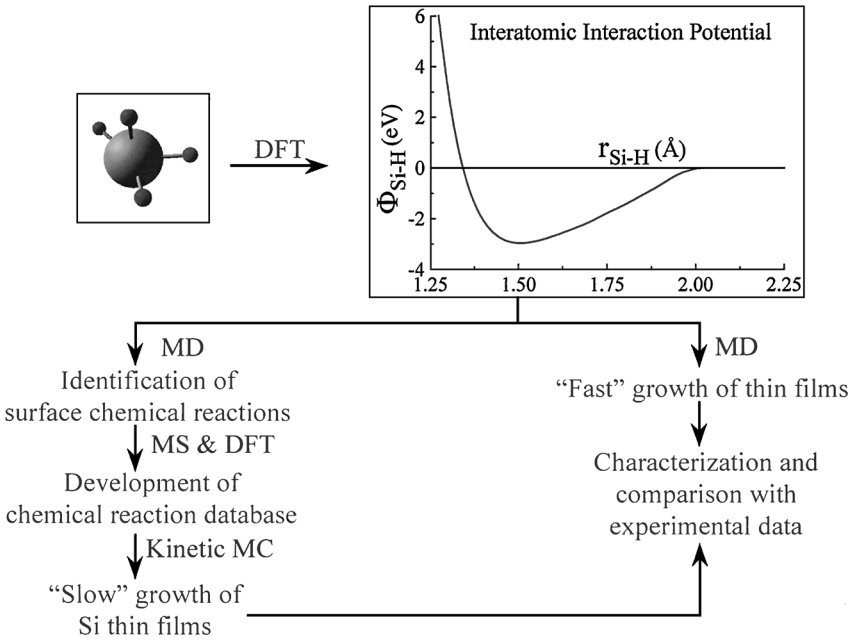

FIG. 1. Diagrammatic outline of the hierarchical approach to modeling plasma–surface interactions in the plasma-enhanced chemical vapor deposition of silicon thin films.

starting point is QM calculation within the framework of density-functional theory (DFT) (Hohenberg and Kohn, 1964; Kohn and Sham, 1965; Payne *et al.,* 1992). DFT-based energy calculations can be used to evaluate the parameters of classical interatomic interaction potentials, which can be used to perform MS, MC, and MD simulations; such *ab initio* potential parametrization is a key to improving the transferability of the classical force field. In Fig. 1, an interatomic potential energy function for Si–H interactions is given as an example of such a parametrization (Ohira *et al.,* 1995).

The classical interatomic potential can be used to carry out MD simulations of "fast" film growth on a substrate. Although the MD growth rates are several orders of magnitude faster than the experimental rates, the MD-deposited films and their surfaces can be characterized in detail and compared with experimental measurements. The main aim of such MD simulations is a fundamental mechanistic understanding and comprehensive identification of chemical reactions that occur on the deposition surfaces, as well as analysis of surface diffusion and relaxation mechanisms. Reaction identification is a very important part of the computational hierarchy: it is the key to interpretation of various experimental observations and construction of the list of reactions needed for KMC simulation of film growth. The identified set of reactions can be analyzed further to contribute

to the process chemical reaction database. Upon identification, the reaction energetics and kinetics can be computed accurately based on DFT calculations that employ a model of the actual surface where the reaction occurs.

KMC modeling of the growth process over coarser time scales requires as input the rates of the surface reactions that have been identified by the MD simulations. These reaction rates can be predicted within the framework of variational rate theory (Voter and Doll, 1985; Hanggi *et al.,* 1990; Makarov and Metiu, 1997) using the computed energy surfaces along the reaction paths. The computed rates for the identified surface reaction processes depend strongly on the local structure and composition of the deposition surface: for Si film growth, the degree of crystallinity and the H coverage of the surface are very important rate determining factors. Simple lattice KMC methods are not appropriate for the study of amorphous or nanocrystalline film growth. In such cases, hybrid off-lattice KMC simulations should be implemented. These MC simulations combine a KMC propagator of the dynamical system over long time scales with an equilibrium MC method for surface relaxation between infrequent events. Such a hybrid KMC approach was implemented recently in the simulation of diamond film growth (Clark *et al.,* 1996a,b).

Executing schedules of film growth dynamical simulations, as outlined in Fig. 1, enables parametric studies toward development of optimal growth strategies. Specification of system parameters that govern plasma–surface interactions may require additional links to gas-phase plasma models and/or plasma diagnostics experiments. Such important parameters include the substrate temperature, the chemical identities and fluxes of species impinging on the deposition surface from the gas phase, the kinetic energies of the impinging species, and the angles of incidence and molecular orientations of the impinging species with respect to the surface.

B. Density-Functional Theory

Computationally efficient *ab initio* quantum mechanical calculations within the framework of DFT play a significant role in the study of plasma–surface interactions. First, they are used to parametrize classical force fields for MD simulations. Second, they provide the quantitative accuracy needed in the development of a chemical reaction database for KMC simulations over long time scales: upon identification of a surface chemical reaction through MD simulation, DFT can be used to address in quantitative detail the reaction energetics and kinetics. Third, DFT-based chemical reaction analysis and comparison with the corresponding predictions of the empirical interatomic potential used in the MD simulations provides further

validation (or insights for further improvement) of the interatomic potential by generating accurate data beyond the data set employed in the potential parametrization.

The choice of the "level of theory," i.e., the type of approximations employed within DFT that determines the level of accuracy of the DFT results, is essential for computationally efficient quantum mechanical analysis of plasma-surface interactions. Such an acceptable level of theory, within a cluster model representation of the surface, has been outlined by Ramalingam *et al.* (1998c). The B3LYP functional (Becke, 1993; Stephens *et al.,* 1994) is used with Gaussian basis sets for the representation of the electronic wavefunctions (Frisch *et al.,* 1984). An effective core potential is employed to represent the $Si1s^2 2s^2 2p^6$ core (Stevens *et al.,* 1984). The cluster that represents the surface includes terminating H atoms that mimic the actual local bonding environment, i.e., Si–Si bonds with bulk Si atoms are replaced by Si–H bonds. The geometry of the cluster atoms is relaxed based on local energy minimization techniques (Payne *et al.,* 1992) and the cluster size effects on the computed energies should be examined by appropriate convergence tests. For analysis of reactions on the Si(001) surface, clusters with four or five atomic layers parallel to the surface plane can be used: the smallest surface model is a four-layer Si_9H_{12} cluster, while a typical size is a five-layer $Si_{23}H_{24}$ cluster. For DFT studies of radical interactions with amorphous surfaces, the necessary cluster model can be constructed using initial configurations taken from the surface region of a classical MD supercell in the vicinity of the reaction site followed by DFT-based structural relaxation of the cluster atoms.

C. Empirical Description of Interatomic Interactions

Several empirical and semiempirical interatomic potentials have been developed for the Si:H system based on extensions and modifications of well-known potentials for Si including up to three-body interactions (Stillinger and Weber, 1985; Biswas and Hamann, 1985; Biswas *et al.,* 1987; Mousseau and Lewis, 1991; Baskes, 1992). Recent atomic-scale simulation work of plasma-surface interactions in the PECVD of Si thin films has been based on an empirical description of interatomic interactions in the Si:H system according to Tersoff's (1986, 1988, 1989) potential for Si, as extended by Ohira and co-workers (1994, 1995, 1996) to incorporate Si–H, H–H, and the corresponding three-body interactions. The extension of the potential to include the presence of hydrogen adopted the Tersoff parametrization to fit results of *ab initio* calculations for the structure and energetics of SiH_x, $x \leq 4$, species in the gas phase (Ohira *et al.,* 1994, 1995, 1996). A similar form of

potential energy functions also was developed by Murty and Atwater (1995). The extended Tersoff potential, U, has the form of a two-body potential with three-body interactions implicitly built in, given by

$$U = \sum_i \sum_{j>i} [a_{ij} V_r(r_{ij}) + b_{ij} V_a(r_{ij})] f_c(r_{ij}), \tag{1}$$

where

$$V_r(r_{ij}) = A_{ij} \exp(-\lambda_{ij} r_{ij}), \qquad V_a(r_{ij}) = -B_{ij} \exp(-\mu_{ij} r_{ij}) \tag{2}$$

$$a_{ij} = \varepsilon_{ij} \left(1 + \beta_i^{n_i} \tau_{ij}^{n_i}\right)^{-1/2n_i}, \qquad b_{ij} = \chi_{ij} \left(1 + \beta_i^{n_i} \xi_{ij}^{n_i}\right)^{-m_i/2n_i} \tag{3}$$

$$\tau_{ij} = \sum_{k \neq i,j} f_c(r_{ik}) \delta_{ik} g(\theta_{ijk}), \qquad \xi_{ij} = \sum_{k \neq i,j} f_c(r_{ik}) \omega_{ik} g(\theta_{ijk}) \times \exp[\sigma_{ik}(r_{ij} - r_{ik})] \tag{4}$$

$$g(\theta_{ijk}) = 1 + \frac{c_i^2}{d_i^2} - \frac{c_i^2}{\left[c_i^2 + (h_i - \cos\theta_{ijk})^2\right]}, \tag{5}$$

and

$$f_c(r_{ij}) = \begin{cases} 1, & r_{ij} < R_{ij} \\ \frac{1}{2} + \frac{1}{2} \cos\left(\frac{\pi(r_{ij} - R_{ij})}{S_{ij} - R_{ij}}\right), & R_{ij} < r_{ij} < S_{ij}, \\ 0, & r_{ij} > R_{ij}. \end{cases} \tag{6}$$

In Eqs. (1)–(6), r_{ij} denotes the interatomic distance between atom i and atom j and θ_{ijk} denotes the angle between the distance vectors $\mathbf{r}_{ij}$ and $\mathbf{r}_{jk}$ subtended at vertex j. Repulsive and attractive interactions are represented in Eqs. (1) and (2) by the potential functions V_r and V_a, respectively. The smooth cutoff function, f_c, limits the range of the potential and reduces the computational cost for energy calculations. The potential is adapted to changes in the local bonding environment by the factors a_{ij} and b_{ij} which multiply in Eq. (1) the repulsive and attractive pair interactions, $V_r(r_{ij})$ and $V_a(r_{ij})$, respectively. These factors represent a measure of bond order and have the appropriate form, Eqs. (3)–(6), to describe the dependence of the local bonding environment on atomic coordination and structure. A complete list of the potential parameters is given by Ohira *et al.* (1996) and Ramalingam *et al.* (1998b).

In spite of the parametrization effort involved in the construction of an empirical interatomic potential, capturing the complexity of plasma–surface interactions poses severe demands on the accuracy and transferability of such a model of interatomic interactions. Thus, careful testing is required prior to using any empirical model for the study of plasma–surface

chemistry. The quantitative accuracy of the interatomic potential of Eqs. (1)–(6) for the study of radical–surface interactions was tested exhaustively through comparisons of its predictions with experimental measurements and results of *ab initio* calculations. Such successful comparisons included the structure and energetics of gas-phase radicals SiH_x ($x = 1, 2, 3$) and clusters Si_nH_m (n > 1), crystalline and amorphous Si bulk phases and surfaces, and mechanisms and energetics of reactions of SiH_x radicals ($x = 1, 2, 3$) with Si surfaces (Ramalingam, 2000; Ramalingam *et al.,* 1998a–c, 1999b, 2000). These comparisons also indicate that the interatomic potential of Eqs. (1)–(6) is capable of quantitative descriptions of radical surface diffusion processes on hydrogen-covered crystalline and amorphous Si surfaces.

D. Methods of Surface Preparation

Careful preparation of the deposition surface is an important step in the study of surface interactions with chemically reactive species from the gas plasma phase. Two types of silicon surfaces are of particular interest: crystalline and amorphous surfaces that are exposed to the chemically reactive plasma species during the PECVD process. Crystalline surfaces, especially the Si(001) surface, are representative of commonly used crystalline substrates (Si wafers) in various experimental studies and practical applications. Amorphous surfaces are representative growth surfaces at later stages of the PECVD process, after an a-Si:H film has been deposited on the substrate.

The crystalline Si(001) surface is prepared in its equilibrium configuration, i.e., a dimerized surface layer according to the (2×1) reconstruction (Yin and Cohen, 1981; Dabrowski and Scheffler, 1992). A bulk crystalline silicon supercell is constructed and a free Si(001) surface is created by removing the periodic boundary conditions in the [001] direction. The atoms on the resulting unreconstructed free surface are given initial displacements toward dimerization of the surface. The system is then mapped onto its minimum-energy configuration using a local nonlinear optimization method, such as a conjugate-gradient algorithm (Gill *et al.,* 1981). Subsequently, the system with the dimerized surface is equilibrated by MD at the temperature of interest to obtain a relaxed Si(001)-(2×1) surface for analysis of plasma–surface interactions. H-terminated Si(001)-(2×1) surfaces (Northrup, 1991) are constructed by introducing a number of hydrogen atoms corresponding to the surface coverage of interest within interaction distance of the Si dangling bonds of the Si(001)-(2×1) surface. The system is relaxed first using a conjugate gradient to minimize its energy and, subsequently, equilibrated at the temperature of interest through MD for several picoseconds.

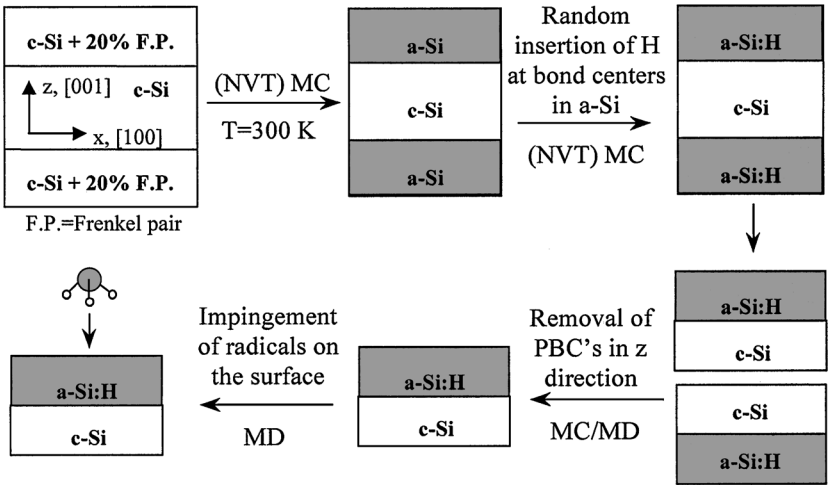

FIG. 2. Schematic illustration of a computational procedure employed to generate a-Si:H/c-Si film/substrate systems through a sequence of steps that involve MC and MD simulations.

The structures of amorphous films and their surfaces vary according to the experimental conditions of film growth. In similar manner, various computational methods can be employed to prepare amorphous films on substrates. One such method (Ramalingam *et al.,* 1998b), based on insights drawn from solid-state amorphization upon irradiation (Barone and Maroudas, 1997), follows the sequence of steps outlined in Fig. 2. First, the volume of a bulk simulation supercell is fixed according to the lattice parameter of crystalline Si (c-Si) at the temperature of interest, as computed through an isothermal–isobaric (NpT) MC simulation. The top and bottom quarters of the c-Si supercell are "damaged" by introduction of Frenkel-pair defects, i.e., pairs of vacancies and self-interstitials removed beyond their recombination range, at concentrations above the critical concentrations for amorphization (Barone and Maroudas, 1997). The resulting structure is equilibrated using canonical (NVT) MC, which yields a layered a-Si/c-Si superstructure with c-Si sandwiched by amorphous silicon (a-Si) layers. Subsequently, hydrogen atoms at a given concentration are introduced randomly at Si–Si bond centers in the amorphized regions of the sample and the system is equilibrated using canonical MC. The MC equilibration consists of a repeated sequence of chemical relaxation and structural relaxation stages. Chemical relaxation involves MC sweeps over the H atoms only, consisting of trial moves of the H atoms for given positions of Si atoms in the a-Si matrix; these moves are accepted or rejected according to the Metropolis criterion (Allen and

Tildesley, 1990). Next, structural relaxation is performed based on MC trial moves of all the atoms in the supercell and acceptance or rejection of the generated configurations according to the Metropolis criterion. This hydrogenation of the a-Si layers results in a layered a-Si:H/c-Si superstructure with structurally stable interfaces. The simulation cell is then cut in half and the periodic boundary conditions (PBCs) are removed in the direction normal to the plane of the a-Si:H/c-Si interface. Additional c-Si atomic layers are placed at the appropriate interlayer distance at the bottom of the resulting simulation cell and are held fixed to simulate contact with an infinite rigid substrate. MC equilibration is used to distribute the hydrogen in the presence of the free surface. Finally, the surface is relaxed further by MD at the temperature of interest.

More commonly, amorphous films on substrates are generated computationally by MD through repeated impingement of species from a gas phase on the growth surface. Such an MD method was used to generate a-Si:H films by impingement of SiH_x radicals ($x = 1, 2, 3$) on an initially H-terminated Si(001)-(2×1) surface for studies of plasma species interactions with the amorphous deposition surface (Ramalingam, 2000; Ramalingam *et al.,* 1998c, 1999b,c). In the MD simulations, the classical equations of motion are integrated using a fifth-order predictor-corrector algorithm, rescaling of the atomic velocities for substrate temperature control, and an integration time step typically of the order of 10^{-16} s; the fine time discretization is dictated mainly by the light mass of the H atoms in the dynamical system. The simulation cells typically include 20 dynamical (001) planes from the initial substrate surface in contact with fixed layers at the bottom of the cell. Typical supercell surface areas are $4a \times 4a$ or larger, where a denotes the Si lattice parameter at the temperature of interest and zero pressure. The impinging radicals are placed initially just beyond the range of interaction with the surface atoms and they are directed normal to the surface, toward randomly chosen surface locations, at random molecular orientations with respect to the surface, and with kinetic energies that correspond to the substrate temperature. For the range of impingement conditions used in these MD simulation studies, the implemented temperature control does not affect either the sequence or the mechanisms of the observed surface chemical reactions. Between successive radical impingement events the system is equilibrated through MD for several picoseconds; a period of 4 ps has been shown to be sufficient to achieve surface relaxation when SiH_3 is used as the sole deposition precursor (Ohira *et al.,* 1995; Ramalingam *et al.,* 1999b). Such MD simulations of film growth require several thousands of impingement events, i.e., a long overall trajectory with a duration of several nanoseconds, and they are particularly demanding computationally. The unique advantage of this procedure is that interactions of radicals can be studied throughout the

simulated growth process with various growth surfaces that are representative of various stages of the actual growth process.

E. Methods of Surface Characterization and Reaction Analysis

Chemical characterization of the computationally generated surfaces and its correlation with the surface structure and composition is an important step in our understanding of the deposition mechanism governed by radical–surface interactions. The surface "reactivity map" introduced by Ramalingam *et al.* (1998a–c, 1999a–c) is an important characterization tool of the surface chemical reactivity with the impinging radical as a function of the location of impingement on the surface. Such maps are surface specific, depend on the molecular orientation of the radical with respect to the surface plane, and are constructed based on a sequence of energy minimization (MS) calculations. Specifically, the total potential energy of the interacting atoms in the simulation supercell is minimized with respect to the atomic coordinates and under the appropriate constraints based on an iterative optimization scheme, such as a conjugate-gradient algorithm (Ramalingam *et al.,* 1998b). The energy gain, ΔE, upon interaction of the surface with the radical approaching the surface in a given (constrained) molecular orientation is calculated over a grid of locations (x, y) on the surface. ΔE provides a measure of the radical reactivity at each surface location: a high energy gain corresponds to a high reactivity of this surface location. This energy gain is expressed with respect to a reference state comprising the surface in the absence of the radical and the free radical. It is defined by

$$\Delta E(x, y) \equiv E_{\mathrm{S-R}}(x, y) - [E_{\mathrm{S}} + E_{\mathrm{R}}], \tag{7}$$

where $E_{\mathrm{S-R}}$ (x, y) is the minimized potential energy of the system with the radical impinged at (x, y) in a specified molecular orientation, E_{s} is the potential energy of the sample with the radical removed beyond interaction range with the surface, and E_{R} is the potential energy of the free radical. The reactivity map is the resulting contour plot of $\Delta E(x, y)$ over the surface. For amorphous film surfaces, systematic analysis of the surface reactivity map also requires detailed surface structural characterization through, e.g., the distribution on the surface of the atomic coordination as a measure of the surface dangling bond density distribution. It should be mentioned that such reactivity maps can be constructed, as a postprocessing characterization step, for a sequence of growth surfaces generated by the MD simulation procedure described in Section II.D.

Upon identification of a reaction as part of an MD trajectory, a similar MS-based procedure is used to derive the energetic progress of the reaction,

the reaction energy landscape, along the corresponding reaction path (Ramalingam *et al.,* 1998c, 1999b). The energy of the atomic configurations along the reaction path is minimized following a local energy minization technique. The computed energies of the reactants, reaction products, and saddle-point configurations are used to obtain reaction energies and thermal activation energy barriers. Such energetic analysis of surface reactions can be performed based on either DFT or an empirical description of interatomic interactions; the DFT analysis is aided significantly by the reaction path identified through MD.

III. Surface Chemical Reactivity with SiH_x Radicals

Plasma-assisted deposition occurs through chemical reactions of species from the plasma with the deposition surface, which may lead to attachment of such species to reactive sites on the surface. In SiH_4-containing plasmas, electron impact dissociation of SiH_4 generates various chemically reactive radicals, such as SiH, SiH_2, and SiH_3, which play key roles in the PECVD process and determine the structure and properties of the deposited films. The structure and chemical composition of a deposition surface exposed to the chemically reactive gas discharge also play an important role in determining the radical–surface reaction mechanisms. The interactions of a radical with a particular surface can be viewed as a set of reactions involving two reactants: the radical and the surface. For a given radical and substrate temperature, the reaction mechanism and products depend on the local structure and chemical composition of the surface in the vicinity of the surface location where the radical impinges, as well as the radical's kinetic energy and molecular orientation with respect to the surface. It should be mentioned that this view of radical–surface interactions also can be useful for lumping reactions into categories for more efficient incorporation of such surface reactions into macroscopic reactor-scale modeling.

A first step toward a fundamental and quantitative understanding of radical–surface interactions is the detailed characterization of well-defined surfaces with respect to their reactivity with isolated radicals impinging from the gas phase at thermal energies. This is a necessary step for understanding the elementary surface chemical mechanisms responsible for film deposition, prior to any analysis of more complex physicochemical processes that take place on a structurally and compositionally evolving surface during PECVD. Among crystalline substrate surfaces, the Si(001) surface is of particular importance for such targeted studies of radical reactivity because of its very frequent use in experimental studies and in engineering applications. Among all

possible orientations of SiH_x, $x = 1, 2, 3$, radicals with respect to the growth surface at normal incidence, two are of particular interest because they represent two limiting cases of high and low reactivity, respectively. In the first one, the Si atom of the radical is closer to the surface, with its dangling bond(s) directed toward the surface: this is termed the Si-down radical configuration. In the second one, the radical impinges on the surface, with its H atom(s) pointing toward the surface, i.e., the Si dangling bond(s) of the radical points away from the surface: this is termed the H-down configuration.

The reactivity of a surface with impinging radicals can be characterized in detail through the reactivity maps discussed above, which are constructed according to Eq. (7) for a given description of interatomic interactions. The computational cost of constructing a reactivity map for a surface is comparable to that for obtaining a short MD trajectory: the cost of the corresponding MS iterative computation for 10^2 grid points on the surface cell and 10^2 iterations for each grid point is comparable to generating an MD trajectory of 10^4 time steps. Although these maps are useful for understanding the reactivity of specific surface locations, reaching conclusions about the overall reactivity of the surface and the reaction mechanisms requires a schedule of MD simulations where the radical is impinged on many different surface locations in different molecular orientations. The reactivity maps can be used as a complementary tool that aids in understanding the trajectory of a radical after it comes within interaction range with the surface. Careful examination of the energy landscapes expressed by the reactivity maps can lead to predictions of even detailed features of the radical dynamics on the surface and can provide insights for designing MD simulation protocols.

A. Structure of Crystalline and Amorphous Silicon Surfaces

The reactivity of a growth surface depends strongly on the distribution of atomic coordination on the surface, which indicates the location of surface atoms with dangling bonds available for reaction. Thus, knowledge of surface structure can yield immediate conclusions on surface reactivity. For example, a pristine Si(001)-(2×1) surface is expected to be highly reactive due to the high density of dangling bonds associated with the dimer atoms: all the atoms of the pristine surface are threefold coordinated, i.e., undercoordinated. The structure of the pristine Si(001)-(2×1) surface (top view) is shown in Fig. 3a (see color insert). Locations 1–6 denote high-symmetry points in the unit cell of the dimerized surface: sites 1 and 2 are between dimers of the same dimer row, 3 is at the center of the Si–Si dimer bond, 4 is right at a dimer atom, and 5 and 6 are sites in the trough between neighboring dimer rows. On the other hand, a Si(001)-(2×1) surface terminated by one

monolayer of H atoms, which is denoted henceforth H:Si(001)-(2×1), is expected to be less reactive: all of the Si atoms on this surface are fully (fourfold) coordinated. The structure of the H:Si(001)-(2×1) surface (top view) is shown in Fig. 3b (see color insert).

The distribution of atomic coordination on amorphous surfaces is more complicated due to the complete disorder and increased corrugation of the surface. For the surfaces of the a-Si:H films generated as outlined in Fig. 2, surface atomic coordination distributions are shown for films with low (16%) and high (50%) hydrogen atomic fractions in Figs. 3c and d (see color insert), respectively. These coordination distributions were computed by calculating the number of bonds formed by the Si atoms at the a-Si:H film surface within a slice of thickness corresponding to two layers of the crystalline substrate; the Si–Si and Si–H bond lengths were used in determining the coordination of the Si surface atoms (Ramalingam *et al.,* 1998b). Figures 3c and d show clearly that the surface of the sample with the lower H concentration is characterized by a higher density of undercoordinated Si atoms than the surface of the film with the higher H concentration; the latter surface is characterized mainly by fourfold coordinated and overcoordinated Si atoms. In general, Figs. 3c and d suggest that the surface of the film with the lower hydrogen content is expected to be overall more reactive than that of the film with the high hydrogen content.

B. Interactions of SiH_x Radicals with Crystalline Silicon Surfaces

Reactivity maps for the interactions of the pristine Si(001)-(2×1) surface with the SiH, SiH_2, and SiH_3 radicals impinging on the surface in the Si-down configuration are shown in Figs. 4a–c (see color insert) respectively. The pristine crystalline surface is indeed very reactive. For all of the three radicals, the most reactive regions lie between the Si dimers in the same row (from site 1 to site 2) and along the Si–Si dimer bond (from site 3 to site 4). The least reactive locations lie in the trough between neighboring dimer rows, i.e., along the line connecting sites 5 and 6. Changes in the molecular orientation of the radicals with respect to the surface plane affect the reactivity of the radicals with the surface. Detailed examination of surface reactivity with the radicals impinging in the H-down configuration has shown that the overall reactivity of the surface is reduced significantly (Ramalingam *et al.,* 1998b, 1999b,c). In these configurations, the dangling bond(s) of the Si atom of the radicals points away from the surface and the presence of the H atom(s) of the radicals reduces or inhibits the Si–Si interaction. As a result, it is observed frequently in MD simulations of radical impingement on the surface in the H-down configuration that the radicals rotate to point their dangling bond(s) toward the surface and react with the surface.

Compared to the pristine Si(001)-(2×1) surface, the H:Si(001)-(2×1) surface has a significantly reduced overall reactivity with the radicals. This is due to the presence of the one monolayer of H atoms on this H-terminated surface that passivates the Si dangling bonds. The corresponding reactivity maps for interactions with the SiH, SiH_2, and SiH_3 radicals impinging on the surface in the Si-down configuration are shown in Figs. 4d,e, and f (see color insert), respectively. In all cases, the center of the Si–Si dimer bond (site 3) is reactive, which suggests the possibility of radical insertion reactions that may involve breaking of the Si–Si dimer bond. For the SiH and SiH_3 radicals, the vicinity of the surface Si–H bond (above site 4) also is reactive: this indicates that H abstraction may be possible through breaking of this Si–H bond upon radical impingement in this vicinity. For SiH_2, regions parallel to the dimers (along the line connecting sites 2, 1, and 6) also exhibit some reactivity. For all of the three radicals, regions between neighboring dimer rows are the least reactive. Again, the surface reactivity with the radicals is reduced significantly when the radicals are directed toward the surface in the H-down configuration (Ramalingam *et al.,* 1998b, 1999b,c).

The detailed interactions between the SiH_x radicals and silicon surfaces can be captured by MD simulations of radical impingement at a grid of locations on the surface with varying radical molecular orientation with respect to the surface. The reactions of SiH with the pristine Si(001)-(2×1) surface can be classified broadly into two classes (Ramalingam *et al.,* 1998b). The radical either adsorbs dissociatively onto the surface or penetrates below the top surface layer into the substrate also resulting in dissociation. The H atom that is released upon radical dissociation becomes an interstitial impurity of the substrate Si lattice and it can migrate rapidly or channel deeper into the substrate. These reactions can be represented as

$$SiH_{(g)} + \text{surface} \rightarrow Si_{(s)} + H_{(i)} \tag{8}$$

and

$$SiH_{(g)} + \text{surface} \rightarrow Si_{(b)} + H_{(i)}, \tag{9}$$

where the subscripts (g), (s), (b), and (i) refer to gas, surface, bulk, and interstitial species, respectively. When SiH attaches to the H:Si(001)-(2×1) surface, the reaction mechanism can be classified into one of two categories (Ramalingam *et al.,* 1998b). The radical either stays intact or adsorbs dissociatively, releasing its H atom into the gas phase. These classes of reactions can be represented as

$$SiH_{(g)} + \text{surface} \rightarrow SiH_{(s)} \tag{10}$$

and

$$SiH_{(g)} + \text{surface} \rightarrow Si_{(s)} + H_{(g)}. \tag{11}$$

The SiH_2 radical attaches to the pristine Si(001)-(2×1) surface at one of five possible adsorption sites (Ramalingam *et al.,* 1999c). These reactions can be represented as

$$SiH_{2_{(g)}} + \_{}_{(s)} \rightarrow SiH_{2_{(s)}}, \tag{12}$$

or

$$SiH_{2_{(g)}} + 2\_{}_{(s)} \rightarrow SiH_{2_{(s)}}, \tag{13}$$

or

$$SiH_{2_{(g)}} + 2Si_{(b)} \rightarrow Si\text{–}SiH_2\text{–}Si_{(s)}, \tag{14}$$

where the additional subscript "$\_$" is used to denote a Si dangling bond on the pristine surface. Reaction (12) leads to a threefold coordinated Si atom in the original SiH_2 radical by attachment to the dangling bond of one of the surface dimer atoms. Reaction (13) leads to fourfold coordination of the Si atom of the radical, as well as two Si atoms on the pristine surface; thus, in general, this reaction is preferred energetically. Reaction (13) represents three mechanisms: the radical may attach to both atoms of a Si–Si dimer with or without breaking the dimer bond, or it may form Si–Si bonds with two Si atoms of adjacent dimer rows and bridge the dimer rows across the trough that separates them. Reaction (14) represents attachment of the radical to two second-layer Si atoms in the trough between dimer rows, which leads to formation of overcoordination defects. However, the energy gain associated with passivating both of the dangling bonds of the radical outweighs the defect formation energy. The reactions of the SiH_2 radical with the H:Si(001)-(2×1) surface can be classified into four categories (Ramalingam *et al.,* 1999c) represented by

$$SiH_{2_{(g)}} + HSi\text{–}SiH_{(s)} \rightarrow HSi\text{–}SiH_2\text{–}SiH_{(s)}, \tag{15}$$

or

$$SiH_{2_{(g)}} + HSi_{(s)} \rightarrow HSi\text{–}SiH_{2_{(s)}}, \tag{16}$$

or

$$SiH_{2_{(g)}} + 2HSi_{(s)} \rightarrow HSi\text{–}SiH_2\text{–}SiH_{(s)}, \tag{17}$$

or

$$SiH_{2_{(g)}} + 2Si_{(b)} \rightarrow Si - SiH_2\text{–}Si_{(s)}. \tag{18}$$

Reaction (15) is an insertion reaction and corresponds to breaking of the Si–Si dimer bond and subsequent bonding of the radical to both atoms of the dimer. Reactions (16) and (17) correspond to attachment of the Si atom of the radical to one and to two surface Si atoms, respectively, and do not result in the breaking of any existing surface Si bonds; in the latter reaction, a second Si–Si bond is formed with a Si atom of an adjacent dimer in the same dimer row. Reaction (18) is similar to Reaction (14) with the pristine surface and represents attachment of the radical to two second-layer Si atoms in the trough between dimer rows.

The SiH_3 radical attaches to the pristine Si(001)-(2×1) surface, more commonly, in one of four absorbed configurations (Ramalingam *et al.,* 1999b). The corresponding reactions can be represented as

$$SiH_{3_{(g)}} + -_{(s)} \rightarrow SiH_{3_{(s)}}, \tag{19}$$

or

$$SiH_{3_{(g)}} + 2-_{(s)} \rightarrow SiH_{3_{(s)}}. \tag{20}$$

Reaction (19) leads to a fourfold coordinated Si atom in the original silyl radical by formation of a Si–Si bond between the radical and one surface atom. Reaction (20) leads to fivefold coordination of the Si atom of the radical and represents three mechanisms: the radical forms two Si–Si bonds by either inserting into a surface dimer through breaking of the dimer bond, or bridging two Si atoms of adjacent dimers in the same dimer row, or forming a bridge between two Si atoms in adjacent dimer rows. Although the Si atom of the radical that adsorbs on the surface through reaction (20) is overcoordinated, the resulting energy gain is substantial due to the passivation of two surface dangling bonds. Two types of reactions may occur upon interaction of the SiH_3 radical with the H:Si(001)-(2×1) surface (Ramalingam *et al.,* 1999b). First, the radical may insert into the surface dimer (at site 3) by breaking the Si–Si dimer bond and forming two Si–Si bonds with the atoms of the dimer. Subsequent relaxation of the adsorbed configuration results in transfer of an H atom from the radical to one of the Si atoms of the original surface dimer. This dissociative adsorption reaction can be represented as

$$SiH_{3_{(g)}} + HSi\text{–}SiH_{(s)} \rightarrow HSi\text{–}SiH_2\text{–}SiH_{2_{(s)}}. \tag{21}$$

In addition, the silyl radical may abstract an H atom from the surface, generate a surface Si dangling bond, and return into the gas phase as a silane molecule. This abstraction reaction can be represented as

$$SiH_{3_{(g)}} + HSi_{(s)} \rightarrow SiH_{4_{(g)}} + Si_{-_{(s)}}. \tag{22}$$

Reactions (21) and (22) are analyzed in some detail in Section IV.

C. Interactions of SiH_x Radicals with Surfaces of Amorphous Silicon Films

The chemical reactivity of a-Si:H film surfaces with impinging radicals from the gas phase is correlated strongly with the local composition of the more complex, completely disordered, corrugated, amorphous surfaces. Reactivity maps for radical–surface interactions are shown in Fig. 5 (see color insert), with the radicals impinging in the Si-down configuration on the surfaces of a-Si:H films that were generated according to the procedure outlined in Fig. 2. Figures 5a,b, and c show the reactivity maps for interactions of the SiH, SiH_2, and SiH_3 radicals, respectively, with the surface of such a film with a 16% H concentration. Clearly, SiH is the most reactive of the three radicals. The correlation between surface atomic coordination (Fig. 3c) and surface reactivity is evident for all three types of interactions: the reactivity, measured as energy gain upon interaction, is higher for surface regions with a higher density of undercoordinated Si atoms that correspond to surface Si dangling bonds. In addition, in a manner similar to the interactions with the crystalline surfaces, the overall reactivity of the amorphous surface is reduced significantly if the radicals impinge on the surface in the H-down configuration with the Si dangling bond(s) of the radicals pointing away from the surface (Ramalingam *et al.,* 1998b, 1999b,c).

Reactivity maps for interactions of the SiH, SiH_2, and SiH_3 radicals with the surface of an a-Si:H film with a 50% H concentration is shown in Figs. 5d, e, and f, respectively. Comparisons with the reactivity maps in Figs. 5a,b, and c, respectively, confirms that the major factor in determining the chemical reactivity of the amorphous surface is its H coverage. Increasing the H concentration in the a-Si:H film leads to an increased H coverage of its surface and, consequently, a decreased density of undercoordinated surface Si atoms due to increased passivation of surface dangling bonds. Again, the reactivity of SiH with this H-rich surface is clearly the highest of the three radicals and the correlation between surface atomic coordination (Fig. 3d) and surface reactivity remains evident. Finally, changing the molecular orientation of the radicals with respect to the surface to the corresponding H-down configurations results in a further significant reduction of the surface reactivity (Ramalingam *et al.,* 1998b, 1999b,c).

In general, the interactions of SiH_x radicals ($x = 1, 2, 3$) with the surfaces of the a-Si:H films are determined strongly by the availability of surface Si dangling bonds and can be classified into three categories, as identified by MD simulations (Ramalingam *et al.,* 1998b, 1999b,c). If the radicals impinge in the vicinity of surface dangling bonds, they adsorb immediately onto the surface, forming strong Si–Si bonds with surface Si atoms. This is frequently the case on surfaces of a-Si:H films with a low H concentration, since the

low H coverage of such surfaces leads to increased density of unpassivated surface dangling bonds. If the radicals impinge on the surface at locations that are completely terminated by H atoms, either they are reflected back into the gas phase or they migrate on the surface until they find energetically favorable surface sites to attach to. Reflection of radicals back into the gas phase is observed frequently for radical impingement on almost completely passivated surfaces of a-Si:H films with a high H concentration.

The above interaction mechanisms are illustrated in Figs. 6a and b, which show two-dimensional projections of MD trajectories of the SiH_3 radical on the surfaces of amorphous films with low (16%) and high (50%) H concentrations, respectively (Ramalingam *et al.,* 1999b). The trajectories are superimposed on the corresponding atomic coordination maps for these surfaces (Figs. 3c and d), for better illustration of the mechanism dependence on H coverage and surface dangling bond density. In Figs. 6a and b, the magnitude of the radical's displacement on the surface from its initial impingement location is indicative of the radical's mobility on the surface. In Fig. 6a, a trajectory is shown of a SiH_3 radical that was impinged near a Si dangling bond on the surface of the film with the low H concentration. Practically immediately (within 1 ps), the radical reacts and adsorbs onto the surface. On the other hand, Fig. 6b shows the trajectory of a SiH_3 radical impinged at a less reactive location on the surface of the film with the high H concentration. The radical migrates on the surface for over 3 ps, until it attaches to an undercoordinated surface Si atom.

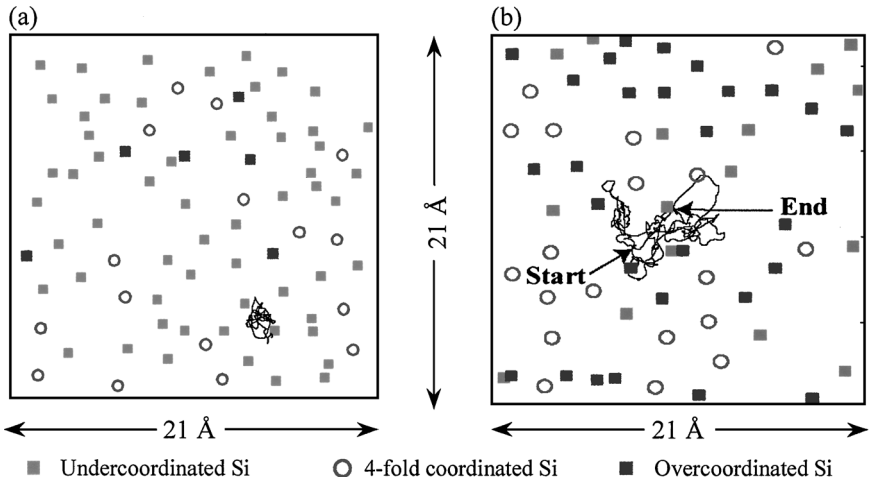

FIG. 6. Two-dimensional projections of SiH_3 center-of-mass trajectories superimposed on the coordination maps of surfaces of a-Si:H films with H concentrations of (a) 16% and (b) 50% (from Ramalingam *et al.,* 1999b).

In general, SiH is the least mobile radical on the surfaces of these a-Si:H films due to its extremely high reactivity with these surfaces that are characterized primarily by surface monohydride species (Ramalingam *et al.,* 1998b). SiH has three Si dangling bonds; as a result, it can often form two Si–Si bonds with the amorphous surface without overly straining any one of its bonds. It is not energetically favorable to break these two Si–Si bonds with simultaneous formation of a Si–Si bond between the surface and the remaining dangling bond of the radical, which limits the mobility of SiH on the surface. On the contrary, the SiH_2 and SiH_3 radicals are very mobile on these amorphous surfaces (Ramalingam *et al.,* 1999b,c). SiH_3 can migrate particularly easily on a-Si:H surfaces with a high H coverage, where most of the surface dangling bonds are passivated by H atoms. On amorphous surfaces with a low H coverage, the SiH_2 radical is generally more mobile than the SiH_3 radical. Although SiH_3 can form a single Si–Si bond with the surface, it must break this bond and form another one with the surface to migrate, hopping from dangling bond to dangling bond on the surface; a relatively high activation energy barrier is associated with this process. In contrast, SiH_2 has two Si dangling bonds, and thus, it can move on the surface by breaking one Si–Si bond with the surface while simultaneously forming another, which is characterized by a lower migration energy barrier.

MD simulations of radical impingement on the surfaces of these a-Si:H films can be used to provide estimates of the overall sticking probability of a radical with these model amorphous surfaces. These overall probabilities correspond to the percentage of reactive events observed in a finite sample of MD trajectories; in the MD simulations, the radicals are directed normal to the surface, in either the Si-down or the H-down configuration, and impinge on the nodes of a grid on the amorphous surface for a-Si:H films of various H concentrations (Ramalingam *et al.,* 1998b, 1999b,c). An alternative approach to calculating sticking probabilities is discussed in Section IV. The estimated overall sticking probabilities from the MD simulations are 96, 70, and 50% for the SiH, SiH_2, and SiH_3 radicals, respectively. SiH is the only silane fragment whose sticking probability on a-Si:H film surfaces has been measured directly in a well-defined experiment; this measured sticking probability is in excess of 94% (Ho *et al.,* 1989), i.e., the computational result is in excellent agreement with the experimental measurement. Due to the specific nature of the films generated by the procedure in Fig. 2 and the relatively small size of the sample employed in the estimation of the above sticking probabilities, detailed comparisons with experimental measurements are not discussed here; more systematic comparisons are discussed below, in Section IV.

IV. Plasma–Surface Interactions during Silicon Film Growth

Our current knowledge of film growth mechanisms by PECVD is inferred largely from macroscopic observations, such as the radical concentrations in the plasma during deposition and the variation of the deposition rates and film properties with the deposition conditions. For example, it is believed widely that the silyl (SiH_3) radical is the dominant precursor in the plasma deposition of a-Si:H films (Robertson and Gallagher, 1986; Matsuda *et al.,* 1990; Abelson, 1993; Perrin *et al.,* 1998). This belief is based largely on the observation that SiH_3 is the most abundant radical in silane plasmas under typical deposition conditions (Abelson, 1993). Dissentions from this view exist and the identity of the primary deposition precursor remains under debate; in general, the deposition precursors depend on the deposition conditions. Several SiH_3–surface reaction mechanisms have been proposed in the experimental literature as important elementary processes that occur during plasma deposition of a-Si:H films. These include abstraction of H atoms from surface sites by impinging SiH_3 radicals, diffusion of SiH_3 radicals on the deposition surface, and reaction between two SiH_3 radicals adsorbed on the surface to form Si_2H_6 (Robertson and Gallagher, 1986; Perrin, 1991; Abelson, 1993; Matsuda, 1998). These radical–surface reaction mechanisms can be examined in detail through atomic-scale simulation of film growth by radical impingement on the growth surface.

Intensive nanosecond-time-scale MD simulations of a-Si:H film growth were carried out recently based on the interatomic potential of Eqs. (1)–(6) (Ramalingam, 2000). These amorphous film growth simulations followed the methodology outlined in Section II. Specifically, the initial configuration consisted of a crystalline silicon substrate with an H:Si(001)-(2×1) surface and the substrate temperature was varied over the range from 500 to 773 K. Motivated by the common belief on the primary importance of the SiH_3 radical as a deposition precursor, special emphasis was placed on the analysis of the MD trajectories of SiH_3 impingement on the growth surface. The MD trajectories for the growth simulations were longer by about three orders of magnitude compared to those analyzed in Section III to characterize the reactivity of well-defined surfaces; thus, these simulations provide a massive amount of atomic-scale information about the film growth mechanisms. In these MD simulations, the surface structure and composition evolve governed by reaction mechanisms between the impinging radicals and the evolving growth surface, which complicates the analysis of these interactions as the growth proceeds.

A. Surface Chemical Reactions during Film Growth

MD simulations of a-Si:H film growth from thermal SiH_3 precursors have revealed a wide range of elementary surface reaction mechanisms that occur on the growth surface (Ramalingam, 2000). These mechanisms can be divided into broad classes that include

- Si incorporation into the grown film either by insertion into surface Si–Si bonds or by direct attachment to surface Si dangling bonds;
- H removal from the growth surface through various abstraction and desorption mechanisms;
- Si–Si bond formation processes by adsorbed species on the surface;
- Si removal from the growth surface, i.e., etching mechanisms that may compete with Si incorporation mechanisms; and
- migration mechanisms of adsorbed mobile surface species that lead to Si transport on the growth surface.

Some of the most important elementary surface chemical reactions are analyzed below, prior to their integration in understanding the complex film deposition mechanism.

One mechanism of Si incorporation into the growing film is dissociative adsorption that involves insertion of the SiH_3 radical into Si–Si bonds (Ramalingam, 2000). At the very initial stages of growth, where the radical impinges on the crystalline H:Si(001)-(2×1) surface, such a mechanism can be represented by reaction (21). The progress of this dissociative adsorption mechanism is illustrated in Fig. 7 through a sequence of snapshots, A, B, C, and D, from MD simulation. In A, the radical is shown impinging in the Si-down configuration on the H:Si(001)-(2×1) surface at the center of the Si–Si surface dimer bond. In B, the radical inserts into the dimer bond: the Si–Si dimer bond is broken and the radical forms Si–Si bonds with both atoms of the original surface dimer. In this configuration, the radical's Si atom is overcoordinated; as a result, one of the Si–Si bonds formed in B is broken, as shown in snapshot C. The MD trajectory reveals that the Si atom of the radical forms bonds alternately, with each of the dimer atoms having its bond with the other broken; this occurs through a hopping process that involves a transition state where the radical is bonded with both of the dimer atoms (Ramalingam *et al.,* 1999b). Upon surface relaxation and at a state where the radical's Si is bonded to only one of the dimer atoms, a hydrogen atom is transferred from the radical to the other atom of the original surface dimer, leading to the formation of a surface dihydride species. The resulting configuration is shown in snapshot D in Fig. 7. This dissociative adsorption mechanism, predicted using the interatomic potential of Eqs. (1)–(6), is fully consistent with DFT-based *ab initio* calculations

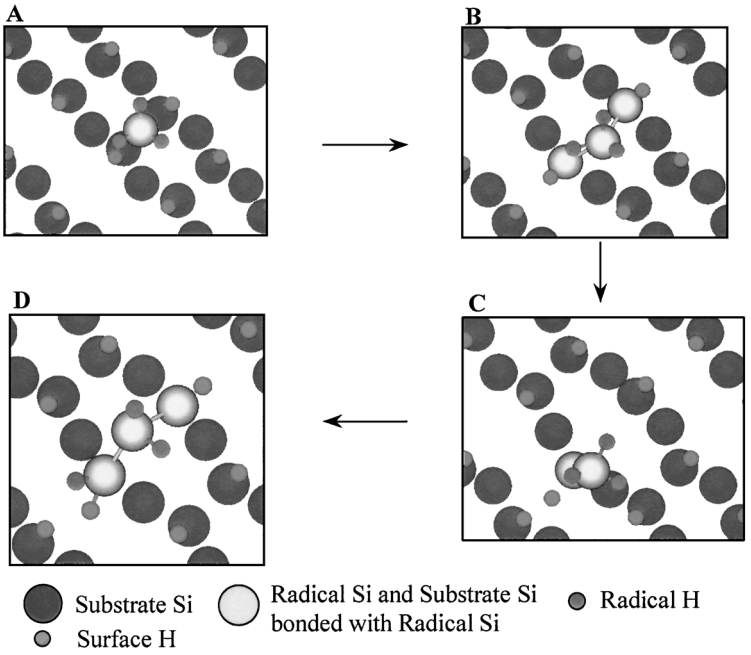

FIG. 7. Sequence of snapshots from MD simulation that illustrate a mechanism of dissociative adsorption of SiH_3 on an H-terminated Si(001)-(2×1) surface (from Ramalingam *et al.,* 1999b).

in terms of its energetic progress along the reaction path and the geometry of the corresponding atomic configurations (Walch *et al.,* 2000).

Several SiH_3 insertion reactions and dissociative adsorption events, where an insertion reaction is followed by H transfer from the radical to the surface, have been observed during MD simulations of a-Si:H film growth (Ramalingam, 2000). This reaction has important implications for the PECVD of Si films. The impinging SiH_3 radical leads to the formation of two SiH_2 species on the deposition surface. In conjunction with other reactions that can produce dihydride species on the surface of a-Si:H films, this SiH_3 dissociative adsorption mechanism can explain the large proportion of surface dihydrides measured on plasma-deposited films (Marra *et al.,* 1998a,b). These MD simulation results also are consistent with the proposal of von Keudell and Abelson (1999) based on their investigation of SiH_3 interactions with a-Si:H film surfaces using infrared spectroscopy. These authors proposed that SiH_3 inserts into the dimer bonds of the crystalline surface during the initial stages of growth and into strained Si–Si bonds on the amorphous growth surface at later stages of deposition.

A very common mechanism of hydrogen removal from the deposition surface during MD simulation of Si film growth is through surface H abstraction by the impinging SiH_3 radical. In the initial stages of growth, such a hydrogen abstraction from the H:Si(001)-(2×1) surface can be represented by reaction (22). This abstraction reaction occurs through an Eley–Rideal mechanism (Ramalingam *et al.,* 1999b), which is illustrated in Fig. 8a. Three MD-generated atomic configurations, A, TS, and B, are shown that capture the radical and the surface at three stages of the abstraction reaction. At A, the SiH_3 radical is impinging on the H:Si(001)-(2×1) surface, but it is still outside interaction range with the surface. TS is the transition-state configuration, where the surface H atom that is being abstracted is bonded both to the Si atom of the impinging silyl radical and to the surface Si atom. At configuration B in Fig. 8a, the Si–H bond of the H atom with the surface is broken and the H atom is attached only to the Si atom of the radical: the

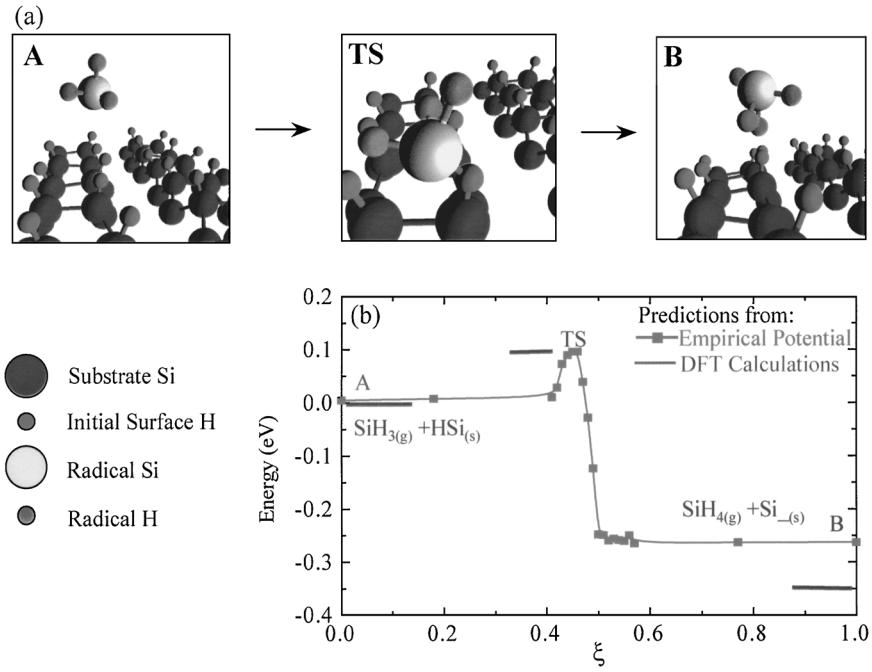

FIG. 8. Hydrogen abstraction by SiH_3 from an H-terminated Si(001)-(2×1) surface (from Ramalingam *et al.,* 1998c, 1999b). (a) Three atomic configurations from MD simulation showing the radical and the surface at different stages of the abstraction reaction; A, TS, and B correspond to the reactant, transition-state, and reaction product configurations. (b) Energetic progress of the reaction along its path as a function of a reaction coordinate, ξ, which expresses a dimensionless Si–H distance between the Si of the radical and the abstracted H.

SiH_4 molecule produced returns to the gas phase. The energetic progress of the Eley–Rideal abstraction along the reaction path is shown in Fig. 8b as a function of a reaction coordinate, ξ. the MD trajectory is followed along the reaction path and the sequence of atomic configurations is mapped onto their local minimum-energy configurations, as discussed in Section II.E. In Fig. 8b, the reactant state, configuration A, is chosen to set the level of zero energy. The reaction coordinate is defined by

$$\xi \equiv \begin{cases} 0, & d_{\mathrm{Si-H}} > d_{\max} \\ \dfrac{d_{\max} - d_{\mathrm{Si-H}}}{d_{\max} - d^{\mathrm{eq}}_{\mathrm{Si-H}}}, & d^{\mathrm{eq}}_{\mathrm{Si-H}} < d_{\mathrm{Si-H}} \le d_{\max}, \\ 1, & d_{\mathrm{Si-H}} \le d^{\mathrm{eq}}_{\mathrm{Si-H}} \end{cases} \tag{23}$$

where $d_{\mathrm{Si-H}}$ is the distance in the optimized configurations between the Si atom of the impinging radical and the H atom that is abstracted from the surface, $d_{\max}$ is the maximum Si–H distance at which the two atoms come within interaction range, and $d^{\mathrm{eq}}_{\mathrm{Si-H}}$ is the equilibrium Si–H bond length in the SiH_4 molecule. The transition-state configuration TS in Fig. 8a is formed at $\xi \approx 0.45$. The reaction energetics in Fig. 8b, predicted according to the interatomic potential of Eqs. (1)–(6), yields an activation energy barrier of 0.095 eV and an exothermic reaction energy of 0.26 eV. These results are in very good agreement with DFT-based pseudopotential cluster calculations, which predict an activation barrier of 0.09 eV and an exothermicity of 0.35 eV (Ramalingam *et al.,* 1998c).

This Eley–Rideal H abstraction reaction occurs not only on the crystalline H:Si(001)-(2×1) surface but also on the deposited a-Si:H film surfaces at later stages of the growth process and can be represented, in general, as

$$SiH_{3_{(g)}} + H_{(s)} \rightarrow SiH_{4_{(g)}} + -_{(s)}. \tag{24}$$

The computed activation energy barriers and exothermicities for reaction (24) on a-Si:H surfaces generated during MD simulation of film growth over the temperature range from 500 to 773 K are in excellent agreement with the energy values computed for the abstraction reaction on the H-terminated crystalline surface (Ramalingam, 2000). This abstraction reaction is very important for the PECVD process, because it provides a mechanism of hydrogen removal from an H-passivated surface. This mechanism generates surface dangling bonds which act as reaction sites on the surface for subsequently impinging SiH_3 radicals.

MD simulations of Si film growth also have revealed a Langmuir–Hinselwood mechanism of hydrogen removal from the growth surface (Ramalingam, 2000). This mechanism involves reaction of an adsorbed SiH_3

species on the surface with surface H to form a weakly adsorbed SiH_4 molecule, which desorbs subsequently into the gas phase. This reaction can be represented as

$$SiH_{3_{(s)}} + H_{(s)} \rightarrow SiH_{4_{(s)}} \rightarrow SiH_{4_{(g)}} + {}_{-(s)}. \tag{25}$$

In reaction (25), the Si atom of the adsorbed silane intermediate is overcoordinated; it is actually highly (sixfold) overcoordinated if the SiH_3 radical has adsorbed through an insertion reaction into a Si–Si surface bond. H transfer is particularly favorable energetically if the H atom is bonded to an overcoordinated surface atom; such coordination defect formation is very common during film growth. The empirical potential of Eqs. (1)–(6) predicts that the H transfer step of reaction (25), from an overcoordinated Si to an inserted SiH_3 radical, occurs with an activation energy barrier of 0.6 eV and leads to an energy gain of 0.45 eV, while the subsequent silane desorption step is endothermic with an energy requirement of 1.4 eV. Reaction (25) is an important surface hydrogen removal mechanism; it occurs on both crystalline and amorphous surfaces, i.e., during both early and later stages of the amorphous film growth process, and it is accelerated substantially by increasing the growth temperature. Other mechanisms of surface H removal that have been studied through MD simulation (Ramalingam, 2000) include abstraction by impinging H atoms on the growth surface and desorption of surface H induced by impingement of energetic species on the surface. Of course, these possible mechanisms of H removal are not active during MD simulation of film growth solely from a thermal SiH_3 precursor.

Hydrogen removal, through either an Eley–Rideal or a Langmuir–Hinselwood mechanism, provides an additional path for Si incorporation into the growing film. As a result, impinging radicals can be incorporated into the growing film through two types of reactions: insertion into a surface Si–Si bond and direct attachment to a surface dangling bond. The energetics of these two reaction classes on a-Si:H films are comparable to those of the corresponding Si adsorption mechanisms on the crystalline Si(001)-(2×1) surface. In all cases, the energy gain upon SiH_3 adsorption is 2.0 eV or higher, as computed by the empirical potential of Eqs. (1)–(6); the energetics of adsorption on the crystalline surface are in agreement with predictions of DFT calculations (Walch *et al.,* 2001). For both reaction mechanisms, the energy gain upon radical adsorption on the amorphous surface is lower by 0.2–0.3 eV than that for radical adsorption on the crystalline surface.

Two adjacent SiH_3 radicals adsorbed on the growth surface react commonly with each other to form a surface disilane (Si_2H_6) species, where one or both of the Si atoms of the radical are overcoordinated (Maroudas *et al.,*

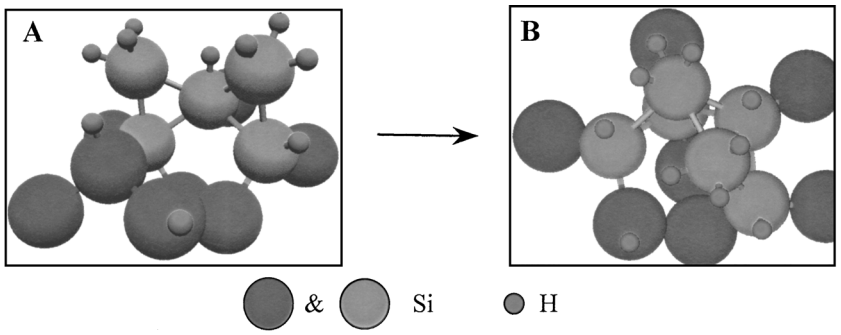

FIG. 9. Surface disilane formation reaction (from Ramalingam, 2000). Two atomic configurations are shown from MD simulation corresponding to the reactants (A) and reaction products (B), respectively.

1999; Ramalingam, 2000). This surface reaction can be represented by

$$SiH_{3(s)} + SiH_{3(s)} \rightarrow Si_2H_{6(s)}. \tag{26}$$

Typically, the two reactant SiH_3 species form a Si–Si bond with a common surface Si atom before they react with each other. The mechanism of such a disilane formation reaction during the initial stages of growth is illustrated in Fig. 9. Configuration A in Fig. 9 shows two adsorbed neighboring SiH_3 radicals with Si–Si bonds with a common surface atom coming within interaction range with each other. Configuration B shows the formation of a Si–Si bond between the two adsorbed radicals producing a $Si_2H_{6(s)}$ species. The Si atoms of $Si_2H_{6(s)}$ and on the surface in the vicinity of the adsorbed species are overcoordinated. This particular mechanism of $Si_2H_{6(s)}$ formation is athermal, i.e., the reaction in Fig. 9 is barrierless, and has an exothermicity of 0.5 eV according to the empirical potential of Eqs. (1)–(6). The high density of coordination defects associated with $Si_2H_{6(s)}$ species favors Si–Si bond breaking processes and leads to easy migration of disilane on the surface and/or desorption from the surface; these thermally activated processes are accelerated at high growth temperatures. Note that desorption of disilane constitutes an etching mechanism, which leads to removal of Si from the surface and begins to compete with Si incorporation as the growth temperature increases. Finally, analysis of MD trajectories has revealed that $Si_2H_{6(s)}$ dissociation, i.e., the reverse of reaction (26), also is possible after its migration on the surface (Ramalingam, 2000).

An important factor in determining the morphology of the amorphous film grown through MD simulations is the observed mobility of the SiH_3 radical on the amorphous growth surface as the deposition proceeds (Ramalingam, 2000). The dynamics of the radical on the surface is

qualitatively similar to those illustrated in Fig. 6 for isolated radical–surface interactions. If the radical impinges on a location of low surface reactivity, its trajectory resembles that in Fig. 6b; surface regions of low reactivity are characterized typically by a high density of fourfold coordinated surface Si atoms. The radical migrates on the surface by a sequence of hops that involve formation and breaking of "weak" Si–Si bonds with fourfold coordinated surface Si atoms; the activation energy barriers associated with this hopping mechanism are very low on the amorphous surface. This sequence of hops continues until the radical finds a reactive site, such as a surface Si dangling bond, and attaches to the surface at this site by forming a "strong" Si–Si bond. Here, the bond strength refers strictly to the bonding energetics, i.e., stronger bonds correspond to greater energy gain upon bond formation. The migration of other species that are weakly adsorbed on the surface, such as $Si_2H_{6(s)}$, also is an important mechanism of Si transport on the growth surface and can affect the morphology of the amorphous film surface.

B. Mechanism of Amorphous Silicon Film Growth

As the MD simulation of a-Si:H film growth proceeds, detailed visualization of the generated MD trajectories is required to analyze the Si bonding patterns and elucidate the complex mechanism of the amorphous network formation process (Ramalingam *et al.,* 2000). Initially, the SiH_3 radicals adsorb on high-symmetry locations of the crystalline substrate surface. When a fractional coverage of the bare crystalline surface is achieved, Si–Si bonds start forming between adjacently adsorbed silyl radicals. Such Si–Si bond formation results in overcoordination of the Si atoms that have attached to the surface, and these newly formed bonds become strained. In addition, the fraction of a monolayer that covers the original growth surface retains largely the crystallinity of the substrate.

As the deposition process continues through radical impingement on the surface, the bonded pairs that were formed during the initial stage of growth evolve to networks of small clusters that consist of three or more adsorbed species bonded with each other. These small clusters form through surface reactions that include Si–Si bond formation, H transfer between adsorbed species, and desorption of species attached to the surface. Cross-linking between the small clusters leads to the formation of larger clusters on the deposition surface. These larger clusters, however, are unstable because their Si–Si bonds are highly strained. As a result, the clusters dissociate through desorption processes accompanied by surface migration of species detached from the clusters. In addition, the high strain in the clusters induces local crystalline-to-amorphous transitions of the bonding network. Some of the

Si–Si bonds on the crystalline substrate surface also break to aid in the accommodation of strain in the clusters of deposited material, resulting in partial loss of the surface structural order. The coordination defects of the Si atoms in the partially amorphized surface are passivated by transport of available H atoms that are bonded to overcoordinated Si atoms in the deposited clusters. These processes determine the structure and composition of the interface that forms between the deposited material and the crystalline substrate. The above relaxation mechanisms stabilize the amorphous pockets on the deposition surface, which grow and coalesce as more radicals arrive from the gas phase to form an amorphous film on the crystalline substrate.

C. Surface Evolution and Film Structural Characterization

The structural evolution of an a-Si:H film deposited by MD at 773 K with SiH_3 as the sole deposition precursor is shown in Fig. 10 (Ramalingam, 2000). Figure 10a shows the profile evolution in the growth direction, z, of

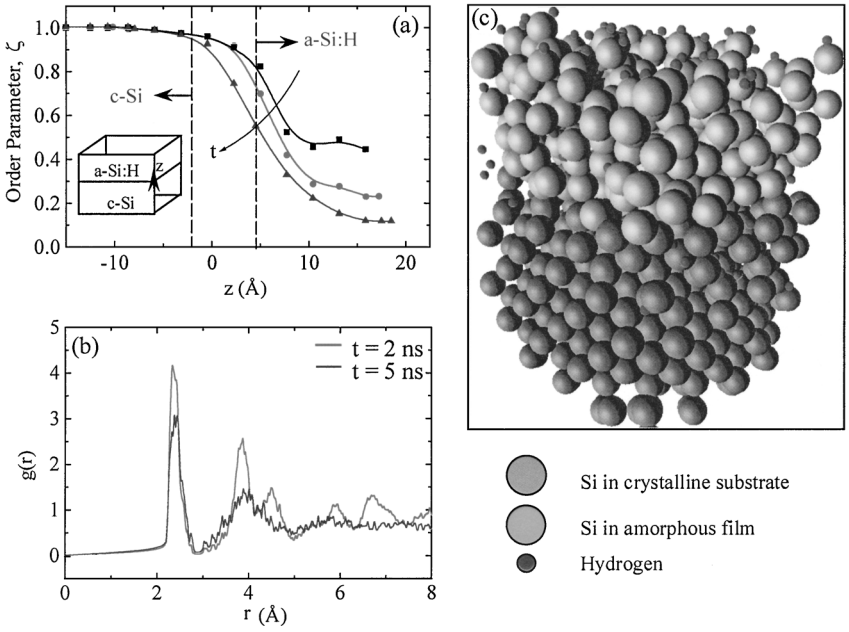

Fig. 10. Structural evolution of an a-Si:H film during its deposition by MD simulation (from Ramalingam, 2000). (a) Profile evolution of the order parameter, ζ, in the direction of growth, z; profiles are shown after 1, 2, and 5 ns, respectively. (b) Si–Si radial distribution function, $g(r)$, after 2 and 5 ns. (c) a-Si:H/c-Si film/substrate configuration after 5 ns of film growth simulation.

an order parameter, ζ, computed over a number of equal thickness slices of the film/substrate system; $z = 0$ corresponds to the initial location of the crystalline substrate surface. The order parameter is defined based on the static structure factor as by Barone and Maroudas (1997); $\zeta = 1$ and $\zeta = 0$ express perfect crystallinity and complete disorder, respectively. Consistently with the film growth mechanism described above, some crystallinity is observed in the deposited film at an early stage of the growth process, which is eventually lost ($\zeta \to 0$) as the growth proceeds resulting in the deposition of an amorphous film. These structural characteristics of the deposited film are elucidated further in Fig. 10b by monitoring the evolution of the Si–Si radial distribution function, $g(r)$, in the film. At early stages of growth, the $g(r)$ peaks indicate that the main crystalline character of the substrate is retained in the deposited film. At later stages of growth, however, the film's short-range order is lost, as expressed by the disappearance of the peaks corresponding to third and higher coordination shells of crystalline (diamond-cubic) Si. A representative a-Si:H/c-Si film/substrate configuration is shown in Fig. 10c; this configuration is obtained after 5 ns of MD simulation of film growth.

Detailed characterization of the deposition surfaces during the film growth simulation elucidate the significant factors that determine the surface reactivity with the impinging radicals (Ramalingam, 2000). Figures 11a,b, and c (see color insert) show the evolution of the growth surface reactivity after MD simulated film growth for 1, 2, and 5 ns, respectively. The reactivity is expressed by the energy gain distribution, as defined by Eq. (7), upon radical–surface interaction with the radical impinging in the Si-down configuration. The evolution of surface reactivity is monitored in conjunction with the evolution of the surface structure and compositional distribution. There is a strong correlation between the surface reactivity distribution and the distribution of H on the surface. Specifically, surface areas which are passivated by H atoms appear as less reactive regions on the reactivity maps. The regions of the surface which are not covered with H atoms are the most reactive: these regions are characterized by the highest densities of surface Si dangling bonds and the lowest density of surface overcoordination defects.

The evolution of the surface roughness during the same MD simulation of film growth is shown in Fig. 12 (see color insert) (Ramalingam, 2000). Figures 12a–c show the evolution of the film height distribution during the simulated growth process. Comparison of Figs. 12a–c with Figs. 11a–c indicates a clear correlation between surface roughness and surface reactivity. Specifically, valleys in the surface topography are preferable regions for concentration of Si dangling bonds, which can be explained by H diffusion away from these valleys to passivate dangling bonds created at the hills of the

surface through, e.g., H abstraction reactions. Such H migration away from the surface valleys is observed within MD time scales, due to the locally very strong driving force for migration toward H-deficient sites on surface hills. In addition, the depth of such valleys on the surface is determined by the presence of mobile species on the surface, which can migrate, "fill" such valleys, and passivate the surface dangling bonds. The surface roughness can be measured by the height–height correlation function, $\eta(r)$ (Barabási and Stanley, 1995). The evolution of $\eta(r)$ during the MD simulation of a-Si:H film growth is shown in Fig. 12c. The local roughness is seen to increase during the initial stages of growth when the deposited film is semicrystalline. At later growth stages, however, the deposited film becomes amorphous, its surface roughness decreases substantially, and $\eta(r)$ is an almost-uniform distribution. Therefore, deposition with SiH_3 as the sole deposition precursor results in a-Si:H films with a remarkably smooth surface. In addition, these films are characterized by a very homogeneous density distribution and a negligible void fraction.

D. Film Surface Composition and Comparison with Experiment

Although MD simulation of film growth from a single thermal precursor does not take into account various surface phenomena that affect the structure and composition of the deposited films, it is worth comparing the MD simulation results with experimental measurements on plasma deposited a-Si:H films. Such comparisons provide insights about the validity of certain assumptions made in the computer simulations.

In the case of the a-Si:H films generated by the MD simulations discussed above (Ramalingam, 2000), comparisons were made of the computed film surface composition with the experimentally measured one in amorphous films deposited by PECVD from SiH_4 containing plasmas without any H_2 dilution; the measurements were based on ATR-FTIR spectroscopy as described by Marra *et al.* (1998a,b). These comparisons are summarized in Fig. 13 for the surface hydride composition at low and high growth temperatures; the SiH_x ($1 \leq x \leq 4$) concentrations are time averaged over several picoseconds after the end of the film growth simulation and are expressed as percentages of the total number of surface silicon hydrides. In Fig. 13a, the growth temperatures in the simulation and the experiment were identical and equal to 500 K. In Fig. 13b the film growth temperature was higher in the simulation (773 K) than in the experiment (640 K); the higher temperature in the simulation was used to accelerate thermally activated surface reactions and speed up the simulated film growth process further. Both experiments and simulations show that SiH_2 is the most abundant surface hydride species

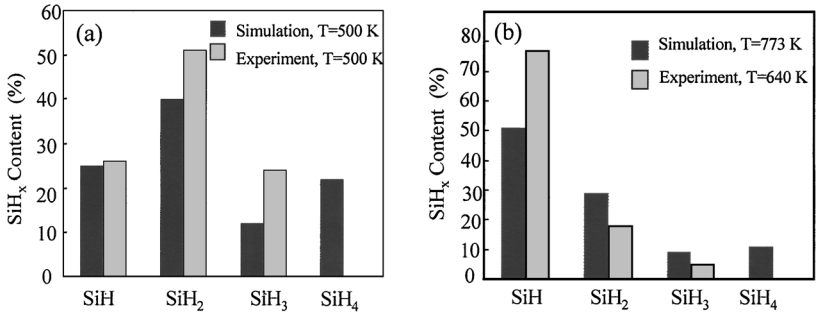

FIG. 13. Comparison of simulated and experimentally measured silicon hydride composition of a-Si:H film surfaces at (a) a low temperature (500 K) and (b) a high temperature (experiment at 640 K, simulation at 773 K).

at 500 K. In contrast, at the higher temperature, the most abundant surface species is SiH: this trend is captured correctly by the MD simulations. The simulations show that SiH is produced through successive thermally activated dissociation of SiH_3 and SiH_2. Furthermore, there is quantitative agreement between the computed surface coverage and the measured coverages at temperatures higher than 430 K (Ramalingam, 2000).

The overall agreement between experimental measurements and MD simulation results indicates that the MD simulations of film growth solely from a thermal SiH_3 precursor have captured several of the key surface reaction mechanisms during a-Si:H film growth and their temperature dependence. However, differences between simulation and experimental results are worth taking into account to improve future simulation strategies. For example, SiH_4 species are not detected in the experiments but they are present on the simulated film surfaces at both temperatures. Such discrepancies are most likely due to unaccounted effects in the MD simulations of energetic ion impingement on the surface and longer surface relaxation between successive radical impingement events. Indeed, silane is weakly bonded to the surface and it is likely to desorb over longer time scales or by ions impinging on the growth surface at kinetic energies higher than thermal.

E. The Role of the Dominant Deposition Precursor

Assuming a dominant precursor for deposition simplifies tremendously the study of plasma–surface interactions. In spite of the oversimplification, it is worth examining the effects on the film structure and composition of growth simulations solely from a given chemically reactive radical. First, direct comparison with experimental data provides an assessment for the

possible role of a given precursor that can be used for more realistic simulation studies even if precise knowledge of impinging species fluxes is not available. More importantly, such studies identify the chemical reactions of this precursor with the surface and elucidate the corresponding mechanisms. Knowledge of such surface chemistry is important prior to examining more complex plasma–surface interactions that involve several chemically reactive species impinging on the surface, both in terms of understanding more complex surface chemistry and in terms of constructing and completing a chemical reaction database.

Several experimental studies have reported reaction probabilities for SiH_3 with Si surfaces during deposition over the range from 5 to 30% (Matsuda *et al.,* 1990; Jasinski, 1993; Nuruddin *et al.,* 1994; Perrin *et al.,* 1998). MD simulations of surface reactivity and film growth have elucidated the importance of the detailed surface structure and chemical composition in determining the corresponding reaction probabilities (Ramalingam *et al.,* 1999b; Ramalingam, 2000). In addition, such atomistic simulation studies can be used to clarify the dependences of reaction probabilities on processing parameters, such as substrate temperature and fluxes and kinetic energies of impinging species on the surface. MD simulations of a-Si:H growth solely from an SiH_3 precursor determined a total reaction probability of 15% from over 1200 impinging radicals on the deposition surface; this probability includes both abstraction and adsorption reactions (Ramalingam, 2000). The reaction probability was found to be practically independent of substrate temperature over the range from 500 to 773 K, which is consistent with experimental data discussed in Section IV.D on the temperature dependence of surface H coverage. These MD simulations do not take into account ion bombardment of the surface, which results in surface dangling bond production and is expected to increase substantially the radical adsorption probability. Indeed MD simulations of energetic particle (25-eV Si atoms) bombardment of films deposited solely from an SiH_3 precursor have shown that such bombardment of the film surface induces hydrogen desorption and generation of surface dangling bonds. The SiH_3 sticking probability was found to be closer to 30% under conditions that lead to high fluxes of energetic ions on the deposition surface (Matsuda *et al.,* 1990; Perrin *et al.,* 1998). However, in the downstream region of a silane discharge, where ion bombardment of the film surfaces is expected to be negligible, the corresponding measured sticking coefficients were less than 10% (Jasinski, 1993). Thus, the experimental observations are fully consistent with the physical understanding obtained from the MD simulations.

For further understanding of the role of SiH_3 as a deposition precursor, a-Si:H films were deposited on crystalline silicon substrates by MD simulation solely from thermal SiH_2 or SiH precursors (Ramalingam, 2000).

Film growth through repeated impingement of SiH_2 on an H:Si(001)-(2×1) surface resulted in a surface that is covered with silicon mono-, di-, and trihydride species, in reasonable agreement with the experimental measurements discussed in Section IV.D; the corresponding total reaction probability of the radical was found to be approximately 40%. On the other hand, when SiH was used as the sole precursor for deposition on the same substrate surface, the resulting surface of the deposited amorphous film contained predominantly silicon monohydrides and some dihydrides; the percentage of the surface dihydride species is too low compared to the experimental value. The computed total reaction probability for SiH was found to be 95% for over 250 radical impingement events on the deposition surface, in excellent agreement with the experimentally measured value (Ho *et al.,* 1989). The surfaces of the films grown from SiH_2 and SiH precursors were rough and the density of structural defects in the films was high: in both cases, the MD deposited films are characterized by a highly inhomogeneous density distribution and a substantial void fraction.

In conclusion, the MD simulations of a-Si:H film growth from the SiH_3, SiH_2, and SiH radicals as the sole deposition precursors support that SiH_3 is the dominant deposition precursor and have elucidated its role in determining the detailed film structure and film surface morphology and composition (Ramalingam, 2000).

F. The Role of Chemically Reactive Minority Species

In spite of the role of the dominant deposition precursor in determining the structure and composition of the deposited film, it is also worth examining the possible roles of minority species that are present at low concentrations in the plasma and are not expected to have significant quantitative contribution to the film growth process. Of particular interest are species that are very reactive with the growth surfaces, such as SiH radicals and small Si_nH_m clusters with $n > 1$. Indeed, such species may have both beneficial and detrimental effects on the structural quality of the deposited film.

Chemically reactive radicals attach to the surface of a-Si:H films either immediately, if they impinge at a chemically reactive location on the surface such as a Si dangling bond, or after some migration on the surface until they find a reactive surface site to attach to. For the SiH radical, detailed analysis of MD trajectories identified a third mechanism of attachment in the case of films with a high hydrogen concentration (Ramalingam *et al.,* 1998a,b). This mechanism is illustrated in Fig. 14a through the evolution of the height coordinate of the radical's center of mass. In trajectories A and B, the radical was impinged on highly reactive locations on an a-Si:H surface with a low

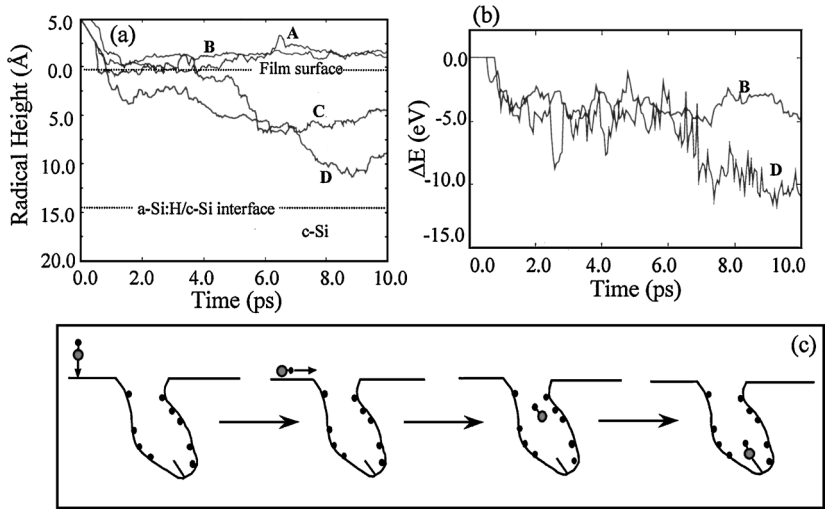

FIG. 14. SiH penetration into a-Si:H films (from Ramalingam *et al.,* 1998a,b). (a) Evolution of the height coordinate of the radical's center of mass for four MD trajectories, A, B, C, and D, of radical impingement on a-Si:H surfaces: in C and D, the radical penetrates into the amorphous film. (b) Energy evolution, $\Delta E(t)$, along trajectories B and D shown in a. (c) Schematic illustration of a common mechanism of radical penetration through an H-passivated nanocavity emanating from the surface of the film.

(16%) and a high (50%) hydrogen concentration in the amorphous film, respectively. In both cases, the radical impinged in the vicinity of Si dangling bonds on the surface, formed strong Si–Si bonds with the corresponding surface atoms and remained attached to the surface for the entire duration of the simulation. In trajectories C and D, however, the radical was directed toward less reactive surface locations of the film with the high hydrogen content; these locations correspond to sites within the lightly colored regions of the reactivity map shown in Fig. 5d, occupied mainly by fourfold and overcoordinated Si atoms. It is evident that in these cases, the radical penetrated into the a-Si:H film. Figure 14b elucidates the energetics of the observed SiH penetration into the a-Si:H film through the evolution of the energy during both MD trajectories, C and D: penetration of the radical into the film is energetically preferable because it leads to Si–Si bond formation due to the availability of Si dangling bonds in the a-Si:H film.

A common mechanism of SiH penetration into hydrogen-rich a-Si:H films is outlined schematically in Fig. 14c (Ramalingam *et al.,* 1998b). This mechanism involves the participation of nanocavities that may be present in the film emanating from the film surface. The presence of such nanocavities is typical of low-quality amorphous films and depend on the deposition

processing conditions; computationally, such nanocavity formation has been observed in various methods of amorphous network generation ranging from defect-induced amorphization to deposition through direct radical impingement. After impingement on an unreactive surface location close to such a nanovoid and short migration on the surface, the SiH radical may enter the nanoscopic cavity; in general, the details of the entrance process depend on the size of the radical, the hydrogen coverage, and the resulting interactions between the nanocavity walls that control the size of the cavity. The walls of the nanocavities are passivated by hydrogen in the form of monohydride, as a result of the high hydrogen content in the film. The radical does not form any Si–Si bonds immediately, but channels through the cavity into the bulk of the film. Typically, the radical penetrates until it reaches the bottom of the cavity, which is characterized by a high Si dangling bond density. As a result, SiH reacts and attaches itself to the bottom surface of the cavity. Contrary to the immediate attachment mechanism, the film penetration mechanism has potentially beneficial effects on the structural quality of the deposited film: it leads to passivation of coordination defects in the film and also contributes to healing larger-scale defects, through filling void space in film nanocavities.

Small neutral and cationic clusters containing several Si atoms also have been shown to be present in silane-containing plasmas (Theil and Powell, 1994; Kessels *et al.,* 1998, 1999a,b;) the cluster size can range up to 9 or 10 Si atoms. Various experimental studies have indicated that clusters containing six Si atoms are particularly stable (Brown *et al.,*1987; Honea *et al.,*1993; Watanabe *et al.,*1997, 1998; Kessels *et al.,*1998, 1999a,b). Approximately 5–10% of the Si incorporated into the film impinges on the surface in the form of such clusters (Kessels *et al.,* 1998, 1999a,b); this percentage is high enough to affect significantly the structure and electronic properties of the entire film. In addition, DFT calculations indicate that $Si_6H_{13}^+$ is the most stable among the $Si_6H_m^+$ clusters (Miyazaki *et al.,* 1996). A significant fraction of cationic clusters is neutralized through collisions with Auger electrons; it should be mentioned, however, that charged clusters have the same framework symmetries as the corresponding neutral clusters (Ragavachari and Logovinsky, 1985). The computed structure of the Si_6H_{13} cluster according to the extended Tersoff interatomic potential, Eqs. (1)–(6), is shown in Fig. 15a; this structure is in excellent agreement with that predicted for $Si_6H_{13}^+$ by *ab initio* calculations (Watanabe *et al.,* 1998). The structure consists of a ring made up of six SiH_2 species connected together by a twofold coordinated hydrogen atom; the presence of this coordination defect suggests the possibility of breaking the ring at the overcoordinated H atom upon interaction of the cluster with the surface. In this discussion, Si_6H_{13} is chosen also as a representative H-rich cluster; the cluster H content is expected to affect the reactivity of the cluster with the surface and the resulting film surface

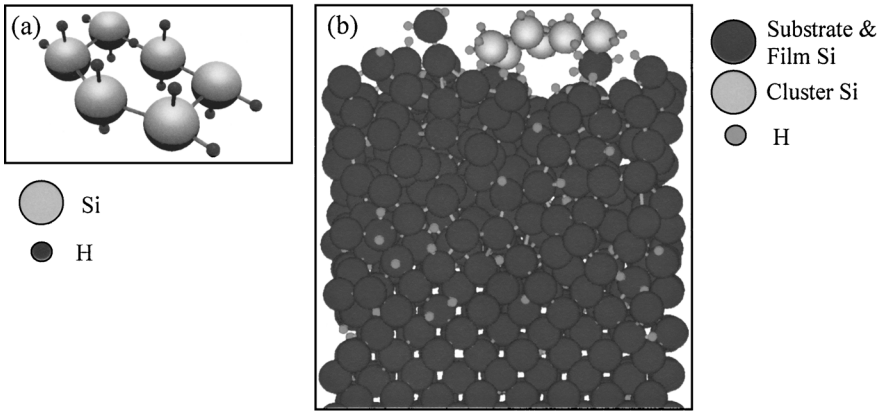

FIG. 15. (a) Computed stable structure of the Si_6H_{13} cluster (from Ramalingam *et al.,* 2000). (b) Representative configuration of an Si_6H_{13} cluster adsorbed on an a-Si:H film surface (from Ramalingam *et al.,* 2000).

structure upon reaction. The qualitative results presented here are expected to apply to both charged and neutral clusters. Furthermore, charged clusters are accelerated toward the surface by strong electric fields in the plasma region; in MD simulations, this is taken into account by impinging the clusters on the surface with appropriately specified kinetic energies.

MD simulations of the interactions of a thermal Si_6H_{13} cluster with a-Si:H film surfaces revealed a high cluster reactivity and cluster-mediated defect formation in the amorphous film. The amorphous films used in the study of the interactions between the cluster and the a-Si:H surfaces were generated by successive impingement (every 4 ps) of thermal SiH_3 radicals on an originally H-terminated Si(001)-(2×1) surface for a substrate temperature of 773 K. The cluster reacts with unit probability and the details of the reaction mechanism depend on the cluster molecular orientation and location of impingement on the surface. In general, the cluster maximizes the number of Si–Si bonds it forms with the surface upon reaction by breaking at the twofold coordinated H atom and undergoing subsequent structural rearrangement (Ramalingam *et al.,* 2001). A possible origin, through cluster–surface interaction, of a deposition-related void defect in the amorphous film is illustrated in Fig. 15b (Ramalingam *et al.,* 2001); this atomic configuration is stable after surface relaxation for over 15 ps. The cluster breaks at the twofold coordinated hydrogen atom forming a five-member ring, attaches to the surface through the formation of three Si–Si bonds with surface Si atoms, and generates a bridge-like structure over a hydrogen passivated trough that already exists on the film surface. This attached cluster structure results in an enclosed void and provides a possible cluster-mediated mechanism of defect formation in the film.

Furthermore, impact of energetic (up to 100-eV) Si_6H_{13} clusters on the a-Si:H film surface can generate additional defects in the film and hydride species on the film surface (Ramalingam *et al.,* 2001). Upon impingement on the film surface, the energetic clusters dissociate. Some of the cluster atoms break Si–Si surface bonds, penetrate into subsurface layers generating overcoordination defects, and form mono-, di-, and trihydride surface species. Therefore, formation of surface hydride species also is possible due to interaction with the deposition surface of minority species, such as Si_nH_m clusters ($n > 1$); traditionally, the presence of surface hydride species in plasma-deposited a-Si:H films has been attributed solely to impinging free SiH_x radicals from the plasma discharge.

V. Summary

Significant progress has been made recently in the fundamental mechanistic and quantitative understanding of radical–surface interactions during plasma deposition processes of Si thin films based on a hierarchical atomic-scale simulation approach. Structurally and chemically well-defined crystalline and amorphous silicon surfaces have been characterized in detail with respect to their reactivity with radicals that are present in silane-containing plasmas. A broad class of chemical reactions that occur on the growth surface during deposition has been identified and analyzed. In addition, model film structures grown on crystalline substrates have been generated computationally and characterized. Furthermore, more realistic input of growth simulation parameters has been identified as an important need to improve the present status of the simulation predictive capabilities.

In spite of these recent advances in the modeling of radical–surface interactions, many important questions on the film growth mechanisms during PECVD remain unanswered and the corresponding chemical reaction database for accurate long-time scale dynamical simulation remains largely incomplete. Future directions for modeling in this area must follow hierarchical simulation approaches, establish direct links to accurate experimental plasma and surface diagnostics, and incorporate additional complexity regarding the identities, fluxes, and energies of radicals impinging on the deposition surface. Addressing these particularly challenging tasks and making use of the ever-increasing capabilities of high-performance computing will enable fully quantitative modeling of plasma deposition processes.

Plasma deposition of semiconductor thin films is just one case of a fundamentally interesting, complex process, where multiscale modeling

(Maroudas and Shankar, 1996; Jensen *et al.,* 1998; Maroudas, 2000) offers a powerful tool toward innovative design for materials property optimization. Advances in the development of multiscale modeling approaches and their implementation for addressing a broad class of problems in electronic materials thin-film processing and reliability presents a unique challenge and opportunity for chemical engineering.

ACKNOWLEDGMENTS

It is a pleasure to acknowledge my long-standing collaboration with Professor Eray S. Aydil at UCSB and the valuable contributions of our graduate student, Shyam Ramalingam, in the area of plasma deposition of silicon thin films. Additional contributions to our research in this area by our students Saravanapriyan Sriraman, Pushpa Mahalingam, Denise Marra, and Sumit Agarwal and our collaborator, Dr. Stephen P. Walch, at NASA Ames Research Center also are gratefully acknowledged. This work was supported by the National Science Foundation, the NSF/DoE Partnership for Basic Plasma Science and Engineering (Award Nos. DMR-9713280 and ECS-0078711), the University of California Energy Institute (Award No. 08960648), the Universities Space Research Association through Cooperative Agreement No. NCC 2-1006 (Award Nos. 8006-001-02, 8008-001-003-001, and 8008-003-005-001), and the Camille & Henry Dreyfus Foundation through a Camille Dreyfus Teacher-Scholar Award.

REFERENCES

Abelson, J. R., Plasma deposition of hydrogenated amorphous silicon: Studies of the growth surface. *Appl. Phys. A Solids Surf.* **56,** 493–512 (1993).

Abraham, F. F., Computational statistical mechanics: Methodology, applications, and supercomputing. *Adv. Phys.* **35,** 1–111 (1986).

Allen, M. P., and Tildesley, D. J., "Computer Simulation of Liquids." Oxford University Press, Oxford, 1990.

Barabási, A.-L., and Stanley, H. E., "Fractal Concepts in Surface Growth." Cambridge University Press, Cambridge, 1995.

Barone, M. E., and Graves, D. B., Chemical and physical sputtering of fluorinated silicon. *J. Appl. Phys.* **77,** 1263–1274 (1995a).

Barone, M. E., and Graves, D. B., Molecular dynamics simulations of direct reactive ion etching of silicon by fluorine and chlorine. *J. Appl. Phys.* **78,** 6604–6615 (1995b).

Barone, M. E., and Maroudas, D., Defect-induced amorphization of crystalline silicon as a mechanism of disordered-region formation during ion implantation. *J. Comp.-Aid. Mater. Des.* **4,** 63–73 (1997).

Baskes, M. I., Modified embedded-atom potentials for cubic materials and impurities. *Phys. Rev. B* **46,** 2727–2742 (1992).

Battaile, C. C., Srolovitz, D. J., and Butler, J. E., Kinetic Monte Carlo method for the atomic-scale simulation of chemical vapor deposition: Application to diamond. *J. Appl. Phys.* **82,** 6293–6300 (1997).

Battaile, C. C., Srolovitz, D. J., and Butler, J. E., Atomic-scale simulations of chemical vapor deposition on flat and vicinal diamond substrates. *J. Crystal Growth* **194,** 353–368 (1998).

Becke, A. D., Density-functional thermochemistry. III. The role of exact exchange. *J. Chem. Phys.* **98,** 5648–5652 (1993).

Biswas, R., and Hamann, D. R., Interatomic potentials for silicon structural energies. *Phys. Rev. Lett.* **55,** 2001–2004 (1985).

Biswas, R., Grest, G. S., and Soukoulis, C. M., Generation of amorphous silicon structures with use of molecular-dynamics simulations. *Phys. Rev. B* **36,** 7437–7441 (1987).

Brown, W. L., Freeman, R. R., Raghavachari, K., and Schluter, M., Covalent group IV atomic clusters. *Science* **235,** 860–865 (1987).

Car, R., and Parrinello, M., Unified approach for molecular dynamics and density-functional theory. *Phys. Rev. Lett.* **55,** 2471–2474 (1985).

Ciccotti, C., Frenkel, D., and McDonald, I. R. (eds.), "Simulations of Liquids and Solids: Molecular Dynamics and Monte Carlo Methods in Statistical Mechanics." North-Holland, Amsterdam, 1987.

Clark, M. M., Raff, L. M., and Scott, H. L., Kinetic Monte Carlo studies of early surface morphology in diamond film growth by chemical vapor deposition of methyl radical. *Phys. Rev. B* **54,** 5914–5919 (1996a).

Clark, M. M., Raff, L. M., and Scott, H. L., Hybrid Monte Carlo method for off-lattice simulation of processes involving steps with widely varying rates. *Comput. Phys.* **10,** 584–590 (1996b).

Crowley, L., Plasma enhanced chemical vapor deposition for flat panel displays. *Solid State Technol.* **35,** 94–97 (1992).

Crowley, M. F., Srivastava, D., and Garrison, B. J., Molecular-dynamics investigation of the MBE growth of Si on Si(100). *Surf. Sci.* **284,** 91–102 (1993).

Dabrowski, J., and Scheffler, M., Self-consistent study of the electronic and structural properties of the clean Si(001)-(2 × 1) surface. *Appl. Surf. Sci.* **56–58,** 15–19 (1992).

Dawnkaski, E. J., Srivastava, D., and Garrison, B. J., Growth of diamond films on a diamond (001)-(2 × 1):H surface by time dependent Monte Carlo simulations. *J. Chem. Phys.* **104,** 5997–6008 (1996).

Fichthorn, K. A., and Weinberg, W. H., Theoretical foundations of dynamical Monte Carlo simulations. *J. Chem. Phys.* **95,** 1090–1096 (1991).

Frisch, M. J., Pople, J. A., and Binkley, J. S., Self-consistent molecular orbital methods. XXV. Supplementary functions for Gaussian basis sets. *J. Chem. Phys.* **80,** 3265–3269 (1984).

Gill, P. E., Murray, W., and Wright, M. H., "Practical Optimization." Academic Press, London, 1981.

Graves, D. B., Plasma processing. *IEEE Trans. Plasma Sci.* **22,** 31–42 (1994).

Graves, D. B., Kushner, M. J., Gallagher, J. W., Garscadden, A., Oehrlein, G. S., and Phelps, A. V., "Database Needs for Modeling and Simulation of Plasma Processing." National Research Council, Panel on Database Needs in Plasma Processing, National Academy Press, Washington, DC, 1996.

Halicioglu, T., and Srivastava, D., Energetics for bonding and detachment steps in etching of Si by Cl. *Surf. Sci.* **437,** L773–L778 (1999).

Hanggi, P., Talkner, P., and Borkovec, M., Reaction rate theory—50 years after Kramers. *Rev. Mod. Phys.* **62,** 251–341 (1990).

Hanson, D. E., Kress, J. D., and Voter, A. F., Reactive ion etching of Si by Cl and Cl_2 ions: Molecular dynamics simulations with comparisons to experiment. *J. Vac. Sci. Technol. A* **17,** 1510–1513 (1999).

Helmer, B. A., and Graves, D. B., Molecular-dynamics simulations of fluorosilyl species impacting fluorinated silicon surfaces with energies from 0.1 to 100 eV. *J. Vac. Sci. Technol. A* **15,** 2252–2261 (1997).

Helmer, B. A., and Graves, D. B., Molecular-dynamics simulations of Ar^+ and Cl^+ impacts onto silicon surfaces: Distributions of reflected energies and angles. *J. Vac. Sci. Technol. A* **16,** 3502–3514 (1998).

Helmer, B. A., and Graves, D. B., Molecular-dynamics simulations of Cl_2^+ impacts onto a chlorinated silicon surface: Energies and angles of the reflected Cl_2 and Cl fragments. *J. Vac. Sci. Technol. A* **17,** 2759–2770 (1999).

Ho, P., Breiland, G., and Buss, R. J., Laser studies of the reactivity of SiH with the surface of a depositing film. *J. Chem. Phys.* **91,** 2627–2634 (1989).

Hohenberg, P., and Kohn, W., Inhomogeneous electron gas. *Phys. Rev.* **136,** B864–B871 (1964).

Honea, E. C., Ogura, A., Murray, C. A., Raghavachari, K., Sprenger, W. O., Jarrold, M. F., and Brown, W. L., Raman spectra of size-selected silicon clusters and comparison with calculated structures. *Nature* **366,** 42–44 (1993).

Jasinski, J. M., Surface loss coefficients for the silyl radical. *J. Phys. Chem.* **97,** 7385–7387 (1993).

Jensen, K. F., Rodgers, S. T., and Venkataramani, R., Multiscale modeling of thin film growth. *Curr. Opin. Solid State Mater. Sci.* **3,** 562–569 (1998).

Kang, H. C., and Weinberg, W. H., Dynamic Monte Carlo with a proper energy barrier: Surface diffusion and two-dimensional domain ordering. *J. Chem. Phys.* **90,** 2824–2829 (1989).

Kessels, W. M. M., van de Sanden, M. C. M., and Schram, D. C., Hydrogen-poor cationic silicon clusters in an expanding argon-hydrogen-silane plasma. *Appl. Phys. Lett.* **72,** 2397–2399 (1998).

Kessels, W. M. M., Leewis, C. M., Leroux, A., van de Sanden, M. C. M., and Schram, D. C., Formation of large positive silicon-cluster ions in a remote silane plasma. *J. Vac. Sci. Technol. A* **17,** 1531–1535 (1999a).

Kessels, W. M. M., Leewis, C. M., van de Sanden, M. C. M., and Schram, D. C., Formation of cationic silicon clusters in a remote silane plasma and their contribution to hydrogenated amorphous silicon film growth. *J. Appl. Phys.* **86,** 4029–4039 (1999b).

Kim, C. K., Kubota, A., and Economou, D. J., Molecular-dynamics simulation of silicon surface smoothing by low-energy argon cluster impact. *J. Appl. Phys.* **86,** 6758–6762 (1999).

Kohn, W., and Sham, L. J., Self-consistent equations including exchange and correlation effects. *Phys. Rev.* **140,** A1133–A1138 (1965).

Kubota, A., and Economou, D. J., A molecular-dynamics simulation of ultrathin oxide films on silicon: Growth by thermal O atoms and sputtering by 100 eV Ar^+ ions. *IEEE Trans. Plasma Sci.* **27,** 1416–1425 (1999).

Kubota, N. A., Economou, D. J., and Plimpton, S. J., Molecular-dynamics simulations of low-energy (25–200 eV) argon ion interactions with silicon surfaces: Sputter yields and product formation pathways. *J. Appl. Phys.* **83,** 4055–4063 (1998).

Limoge, Y., and Bocquet, L., Monte Carlo simulation in diffusion studies: Time scale problems. *Acta Metall.* **36,** 1717–1725 (1988).

Makarov, D. E., and Metiu, H., The reaction rate constant in a system with localized trajectories in the transition region: Classical and quantum dynamics. *J. Chem. Phys.* **107,** 7787–7799 (1997).

Maroudas, D., Multi-scale modeling of hard materials: Challenges and opportunities for chemical engineering. *AIChE J.* **46,** 878–882 (2000).

Maroudas, D., and Brown, R. A., Calculation of thermodynamic and transport properties of intrinsic point defects in silicon. *Phys. Rev. B* **47,** 15562–15577 (1993).

Maroudas, D., and Shankar, S., Electronic materials process modeling. *J. Comp.-Aid. Mater. Des.* **3,** 36–48 (1996).

Maroudas, D., Ramalingam, S., and Aydil, E. S., Atomic-scale modeling of plasma-surface interactions in the PECVD of silicon. In "Fundamental Gas-Phase and Surface Chemistry of Vapor-Phase Materials Synthesis," (Allendorf, M. D., Zachariah, M. R., Mountziaris, T. J., and McDaniel, A. H., Eds.), Electrochemical Society Proceedings Series, Vol. 98-23, Electrochemical Society, Pennington, NJ, 1999, pp. 179–190.

Marra, D. C., Edelberg, E. A., Nanone, R. L., and Aydil, E. S., Silicon hydride composition of plasma-deposited hydrogenated amorphous and nanocrystalline silicon films and surfaces. *J. Vac. Sci. Technol. A* **16,** 3199–3210 (1998a).

Marra, D. C., Edelberg, E. A., Nanone, R. L., and Aydil, E. S., Effect of H_2 dilution on the surface composition of plasma deposited silicon films from SiH_4. *Appl. Surf. Sci.* **133,** 148–151 (1998b).

Matsuda, A., Plasma and surface reactions for obtaining low defect density amorphous silicon at high growth rates. *J. Vac. Sci. Technol. A* **16,** 365–368 (1998).

Matsuda, A., Nomoto, K., Takeuchi, Y., Suzuki, A., Yuuki, A., and Perrin, J., Temperature dependence of the sticking and loss probabilities of silyl radicals on hydrogenated amorphous silicon. *Surf. Sci.* **227,** 50–56 (1990).

Miyazaki, T., Uda, T., Stich, I., and Terakura, K., Theoretical study of the structural evolution of small hydrogenated silicon clusters: Si_6H_x. *Chem. Phys. Lett.* **261,** 346–352 (1996).

Mousseau, N., and Lewis, L. J., Dynamical models of hydrogenated amorphous silicon. *Phys. Rev. B* **43,** 9810–9817 (1991).

Murty, M. V. R., and Atwater, H. A., Empirical interatomic potential for Si-H interactions. *Phys. Rev. B* **51,** 4889–4893 (1995).

Northrup, J. E., Structure of Si(001)H: Dependence on the H chemical potential. *Phys. Rev. B* **44,** 1419–1422 (1991).

Nuruddin, A., Doyle, J. R., and Abelson, J. R., Surface reaction probability in hydrogenated amorphous silicon growth. *J. Appl. Phys.* **76,** 3123–3129 (1994).

Ohira, T., Inamura, T., and Adachi, T., Molecular dynamics simulation of hydrogenated amorphous silicon with Tersoff potential. *Mater. Res. Soc. Symp. Proc.* **336,** 177–182 (1994).

Ohira, T., Ukai, O., Adachi, T., Takeuchi, Y., and Murata, M., Molecular-dynamics simulations of SiH_3 radical deposition on hydrogen-terminated Si(100) surfaces. *Phys. Rev. B* **52,** 8283–8287 (1995).

Ohira, T., Ukai, O., Noda, M., Takeuchi, Y., and Murata, M., Molecular-dynamics simulations of hydrogenated amorphous silicon thin-film growth. *Mater. Res. Soc. Symp. Proc.* **408,** 445–450 (1996).

Pal, S., and Fichthorn, K. A., Accelerated molecular dynamics of infrequent events. *Chem. Eng. J.* **74,** 77–83 (1999).

Payne, M. C., Teter, M. P., Allan, D. C., Arias, T. A., and Joannopoulos, J. D., Iterative minimization techniques for ab initio total-energy calculations: Molecular dynamics and conjugate gradients. *Rev. Mod. Phys.* **64,** 1045–1097 (1992).

Perrin, J., Plasma and surface reactions during a-Si:H film growth. *J. Non-Cryst. Solids* **137–138,** 639–644 (1991).

Perrin, J., Shiratani, M., Kae-Nune, P., Videlot, H., Jolly, J., and Guillon, J., Surface reaction probabilities and kinetics of H, SiH_3, Si_2H_5, CH_3, and C_2H_5 during deposition of a-Si:H and a-C:H from H_2, SiH_4, and CH_4 disharges. *J. Vac. Sci. Technol. A* **16,** 278–289 (1998).

Proud, J. M., Gottscho, R. A., Bondur, J., Garscadden, A., Heberlein, J., Herb, G. K., Kushner, M. J., Lawler, J., Lieberman, M., Mayer, T. M., Phelps, A. V., Roman, W., Sawin, H. H., Winters, H., Perepezko, J., Hazi, A. U., Kennel, C. F., and Gerardo, J., "Plasma Processing of Materials: Scientific Opportunities and Technological Challenges." National Research Council, Report on Processing, National Academy Press, Washington, DC, 1991.

Raghavachari, K., and Logovinsky, V., Structure and bonding in small silicon clusters. *Phys. Rev. Lett.* **55,** 2853–2856 (1985).

Ramalingam, S., "Plasma-Surface Interactions in Deposition of Silicon Thin Films: An Atomic-Scale Analysis," Ph.D. thesis, University of California, Santa Barbara, 2000.

Ramalingam, S., Maroudas, D., and Aydil, E. S., Atomistic simulation of SiH interactions with silicon surfaces during deposition from silane containing plasmas. *Appl. Phys. Lett.* **72,** 578–580 (1998a).

Ramalingam, S., Maroudas, D., and Aydil, E. S., Interactions of SiH radicals with silicon surfaces: An atomic-scale simulation study. *J. Appl. Phys.* **84,** 3895–3911 (1998b).

Ramalingam, S., Maroudas, D., Aydil, E. S., and Walch, S. P., Abstraction of hydrogen by SiH_3 from hydrogen-terminated Si(001)-(2×1) surfaces. *Surf. Sci.* **418,** L8–L13 (1998c).

Ramalingam, S., Maroudas, D., and Aydil, E. S., Visualizing radical-surface interactions in plasma deposition processes: Reactivity of SiH_3 radicals with Si surfaces. *IEEE Trans. Plasma Sci.* **27,** 104–105 (1999a).

Ramalingam, S., Maroudas, D., and Aydil, E. S., Atomistic simulation study of the interactions of SiH_3 radicals with silicon surfaces. *J. Appl. Phys.* **86,** 2872–2888 (1999b).

Ramalingam, S., Mahalingam, P., Aydil, E. S., and Maroudas, D., Theoretical study of the interactions of SiH_2 radicals with silicon surfaces. *J. Appl. Phys.* **86,** 5497–5508 (1999c).

Ramalingam, S., Aydil, E. S., and Maroudas, D., Molecular-dynamics study of the interactions of small thermal and energetic silicon clusters with crystalline and amorphous silicon surfaces. *J. Vac. Sci. Technol. B* **19,** 634–644 (2001).

Randhawa, H., Review of plasma-assisted deposition processes. *Thin Solid Films* **196,** 329–349 (1991).

Rapaport, D. C., "The Art of Molecular Dynamics Simulation." Cambridge University Press, Cambridge, 1998.

Reif, R., Plasma enhanced chemical vapor deposition of thin films for microelectronics processing. In "Handbook of Plasma Processing Technology: Fundamentals, Etching, Deposition, and Surface Interactions," (Rossnagel, S. M., Cuomo, J. J., and Westwood, W. D., Noyes, Eds.), Park Ridge, NJ, 1990.

Ricca, A., and Musgrave, C. B., Theoretical study of the Cl-passivated Si(111) surface. *Surf. Sci.* **430,** 116–125 (1999).

Robertson, R., and Gallagher, A., Mono- and di-silicon radicals in silane-argon DC discharges. *J. Appl. Phys.* **59,** 3402–3411 (1986).

Schoolcraft, T. A., and Garrison, B. J., Initial stages of etching of the Si(001)-(2×1) surface by 3.0-eV normal incident fluorine atoms: A molecular-dynamics study. *J. Am. Chem. Soc.* **113,** 8221–8228 (1991).

Sinke, W. C., The photovoltaic challenge. *MRS Bull.* **18**(10), 18–20 (1993).

Smith, D. L., "Thin Film Deposition." McGraw–Hill, New York, 1996.

Srivastava, D., and Garrison, B. J., Growth mechanisms of Si and Ge epitaxial films on the dimer reconstructed Si(100) surface via molecular dynamics. *J. Vac. Sci. Technol. A* **8,** 3506–3511 (1990).

Srivastava, D., and Garrison, B. J., Modeling the growth of semiconductor epitaxial films via nanosecond time scale molecular-dynamics simulations. *Langmuir* **7,** 683–692 (1991).

Srivastava, D., Halicioglu, T., and Schoolcraft, T. A., Fluorination of Si(001)-(2×1) surface near step edges: A mechanism for surface defect induced etching. *J. Vac. Sci. Technol. A* **17,** 657–661 (1999).

Stephens, P. J., Devlin, F. J., Chabalowski, C. F., and Frisch, M. J., Ab initio calculation of vibrational absorption and circular dichroism spectra using density functional force fields. *J. Phys. Chem.* **98,** 11623–11627 (1994).

Stevens, W. J., Basch, H., and Krauss, M., Compact effective potentials and efficient shared exponent basis sets for the first- and second-row atoms. *J. Chem. Phys.* **81,** 6026–6033 (1984).

Stillinger, F. H., and Weber, T. A., Computer simulation of local order in condensed matter phases of silicon. *Phys. Rev. B* **31,** 5262–5271 (1985).

Tersoff, J., New empirical model for the structural properties of silicon. *Phys. Rev. Lett.* **56,** 632–635 (1986).

Tersoff, J., New empirical approach for the structure and energy of covalent systems. *Phys. Rev. B* **37,** 6991–7000 (1988).

Tersoff, J., Modeling solid state chemistry: Interatomic potentials for multicomponent systems. *Phys. Rev. B* **39,** 5566–5568 (1989).

Theil, J. A., and Powell, G., The effects of He plasma interactions with SiH_4 in remote plasma enhanced chemical vapor deposition. *J. Appl. Phys.* **75,** 2652–2666 (1994).

Von Keudell, A., and Abelson, J. R., Direct insertion of SiH_3 radicals into strained Si–Si surface bonds during plasma deposition of hydrogenated amorphous silicon films. *Phys. Rev. B* **59,** 5791–5798 (1999).

Voter, A. F., A method for accelerating the molecular-dynamics simulation of infrequent events. *J. Chem. Phys.* **106,** 4665–4677 (1997a).

Voter, A. F., Hyperdynamics: Accelerated molecular dynamics of infrequent events. *Phys. Rev. Lett.* **78,** 3908–3911 (1997b).

Voter, A. F., Parallel replica method for dynamics of infrequent events. *Phys. Rev. B* **57,** R13985–R13988 (1998).

Voter, A. F., and Doll, J. D., Dynamical corrections to transition state theory for multistate systems: Surface cell diffusion in the rare event regime. *J. Chem. Phys.* **82,** 80–92 (1985).

Walch, S. P., Ramalingam, S., Aydil, E. S., and Maroudas, D., Mechanisms and energetics of dissociative adsorption of SiH_3 on the hydrogen-terminated Si(001)-(2×1) surface. *Chem. Phys. Lett.* **329,** 304–310 (2000).

Walch, S. P., Ramalingam, S., Sriraman, S., Aydil, E. S., and Maroudas, D., Mechanisms and energetics of SiH_3 adsorption on the pristine Si(001)-(2×1) surface. *Chem. Phys. Lett.,* in press (2001).

Watanabe, M. O., Murakami, H., Miyazaki, T., and Kanayama, T., Three types of stable structures of hydrogenated silicon clusters. *Appl. Phys. Lett.* **71,** 1207–1209 (1997).

Watanabe, M. O., Kawashima, N., and Kanayama, T., Ambient gas dependence of hydrogenated silicon clusters grown in an ion trap. *J. Phys. D Appl. Phys.* **31,** L63–L66 (1998).

Weakliem, P. C., and Carter, E. A., Surface chemical reactions studied via ab initio-derived molecular-dynamics simulations: Fluorine etching of Si(100). *J. Chem. Phys.* **98,** 737–745 (1993).

Yin, M. T., and Cohen, M. L., Theoretical determination of surface atomic geometry: Si(001)-(2×1). *Phys. Rev. B* **24,** 2303–2306 (1981).